sustainability

MDPI

Article

Geoinformatic Analysis of Rainfall-Triggered Landslides in Crete (Greece) Based on Spatial Detection and Hazard Mapping

Athanasios V. Argyriou [1,2,*], Christos Polykretis [1], Richard M. Teeuw [2] and Nikos Papadopoulos [1]

[1] Laboratory of Geophysical—Satellite Remote Sensing & Archaeo-Environment (GeoSat ReSeArch), Institute for Mediterranean Studies (IMS), Foundation for Research & Technology Hellas (FORTH), 74100 Rethymno, Greece; polykretis@ims.forth.gr (C.P.); nikos@ims.forth.gr (N.P.)

[2] Centre for Applied Geosciences, School of Earth and Environmental Sciences, University of Portsmouth, Portsmouth PO1 3QL, UK; richard.teeuw@port.ac.uk

* Correspondence: nasos@ims.forth.gr; Tel.: +30-283-110-6021

Abstract: Among several natural and anthropogenic conditioning factors that control slope instability, heavy rainfall is a key factor in terms of triggering landslide events. In the Mediterranean region, Crete suffers the frequent occurrence of heavy rainstorms that act as a triggering mechanism for landslides. The Mediterranean island of Crete suffers from frequent occurrences of heavy rainstorms, which often trigger landslides. Therefore, the spatial and temporal study of recent storm/landslide events and the projection of potential future events is crucial for long-term sustainable land use in Crete and Mediterranean landscapes with similar geomorphological settings, especially with climate change likely to produce bigger and more frequent storms in this region. Geoinformatic technologies, mainly represented by remote sensing (RS) and Geographic Information Systems (GIS), can be valuable tools towards the analysis of such events. Considering an administrative unit of Crete (municipality of Rethymnon) for investigation, the present study focused on using RS and GIS-based approaches to: (i) detect landslides triggered by heavy rainstorms during February 2019; (ii) determine the interaction between the triggering factor of rainfall and other conditioning factors; and (iii) estimate the spatial component of a hazard map by spatially indicating the possibility for rainfall-triggered landslides when similar rainstorms take place in the future. Both landslide detection and hazard mapping outputs were validated by field surveys and empirical analysis, respectively. Based on the validation results, geoinformatic technologies can provide an ideal methodological framework for the acquisition of landslide-related knowledge, being particularly beneficial to land-use planning and decision making, as well as the organization of emergency actions by local authorities.

Keywords: geoinformatics; remote sensing; GIS; landslides; rainfall; weight of evidence; Crete

Citation: Argyriou, A.V.; Polykretis, C.; Teeuw, R.M.; Papadopoulos, N. Geoinformatic Analysis of Rainfall-Triggered Landslides in Crete (Greece) Based on Spatial Detection and Hazard Mapping. *Sustainability* **2022**, *14*, 3956. https://doi.org/10.3390/su14073956

Academic Editor: Marc A. Rosen

Received: 8 February 2022
Accepted: 23 March 2022
Published: 27 March 2022

1. Introduction

Landslides are one of the most dangerous and destructive natural hazards [1]. Several natural and anthropogenic conditioning factors can increase slope instability, ensuing landslide activity, sometimes with devastating impacts on human life and the environment [2]. These factors are diverse, dynamic and of variable importance from one region to another. Generally, they can be subdivided into two main groups: (i) those triggering a landslide; and (ii) those having a causal role on landslide occurrence [3]. Landslides can be triggered by natural processes such as earthquakes and extreme rainfall events, and anthropogenic factors such as road construction, deforestation, urban expansion and agricultural activity [4]. Intense rainfall is a key factor that can accelerate the triggering of landslides, especially sudden landslides without any previous evidence of significant slope instability, due to pore pressure [5]. Local government planners and emergency managers need to be aware of where landslide events can occur, so that they can implement mitigation measures to save lives and minimize damages.

The impact of the causal factors on the occurrence of landslides is often not well constrained or examined [6]. There are numerous studies exploring landslide occurrence according to various common factors (e.g., slope, rainfall, land use, road proximity and fault proximity), but a rarely considered factor is the presence of agricultural terracing [7,8]. Agricultural terracing can potentially be an important factor in slope instability, but it is rarely acknowledged as a causal factor in landslide-related studies [9]. The construction of terraces on hilly terrain provides flat ground for cultivation, and is a farming method that has been used for thousands of years, especially in the Mediterranean region [10,11]. For centuries, agriculture terraces have characterized the landscapes of Greece, Italy, France, Portugal and Spain. Agricultural terracing influences hydrological and geomorphological processes, especially the associated abrupt changes between rugged terrain and flat cultivated land, artificial drainage channels and irrigation practices, as well as terrace abandonment [12,13].

With any landslide, it is important to understand the nature of the individual factors and their importance in the occurrence of slope failures. Geoinformatic technologies, mainly represented by remote sensing (RS) and geographic information systems (GIS), can be valuable tools, enabling the examination and evaluation of factors associated with landslide activity. Various studies have used empirical methods to analyze the relationship between rainfall and landslide activity, but they are usually independent of associated variables such as lithology, land use and geomorphological processes [14]. A global problem is often the sparse network of meteorological stations—generally adequate for national-scale studies but inadequate for district-scale analysis—which can limit estimation of the areal and temporal distribution of rainfall in case studies of landslide disasters. Satellite-based earth observation (EO) and environmental monitoring systems (e.g., GOES, MODIS, GPM, CHRS) can offer a better overview of rainfall distribution and facilitate analysis of their interrelationship with other factors associated with landslide occurrence, as well as informing local pre-event situational awareness [8].

The aim of this study was to highlight the significant contribution of geoinformatic technologies and tools to the analysis of rainfall-triggered landslides. Considering a case study from the island of Crete, Greece, RS and GIS-based approaches have been used here to: (i) detect landslides triggered by heavy rainfall events in February 2019; (ii) determine the interaction between the triggering factor of rainfall and other causal environmental and anthropogenic factors; and (iii) extract spatial predictions for the potential occurrence of rainfall-triggered landslides in the future by assessing and mapping landslide hazards.

2. Study Area

Crete Island is located in the southern part of Greece (Figure 1a) and is 160 km from the Greek mainland. With an extent of 8261 km^2, length of 260 km, and width ranging from 12 km to 57 km, Crete is the largest Greek island and the fifth largest in the Mediterranean [15]. It is a well-known tectonically active region that lies within the outer fore-arc active subduction zone of the Hellenic arc, with an observed co-seismic uplift up to 9 m on its south-western part [16,17]. In general, various background studies have investigated the tectonic activity, geological and morphological status of western Crete, highlighting the complex geology and wide range of processes and materials that have shaped its landscape [18–20].

During February 2019, the western Crete region, including the municipality of Rethymnon, was severely impacted by storms and unprecedented heavy rainfall which caused fatalities, infrastructure damages and triggered numerous landslides within a few days [3]. For this reason, the present study focuses on this specific administrative unit of Crete. The municipality is located in northern Crete (Figure 1b) and has an extent of about 400 km^2. According to the 2011 census maintained by the Hellenic Statistical Authority, its official population is 55,525 inhabitants [21]. Geologically, the region is characterized by Neogene and Quaternary sedimentary formations (Figure 1c). Slope instability occurs where specific litho-stratigraphic units are present, notably marls, mudstones and phyllites which can lose

their shear strength due to weathering [22,23]. The mudstones mainly correspond to clay minerals with amounts ranging from 30% to 50% and different stabilized strengths [24]. Moreover, outcrops characterized as "Phyllites–Quartzites" comprise three different litho-stratigraphic units representing the phyllitic base of western Crete [25]. Slope instability can be accelerated when there is a heavy rainfall in a short-term period (i.e., many hours to a few days) especially in land use areas with soil prone to degradation and erosion [26]. In such situations, there is an increase in the weight of hillside rock mass due to water accumulation, with cracks and fissures in the soil giving surface water access to the regolith, resulting in sudden landslide occurrences [3,4].

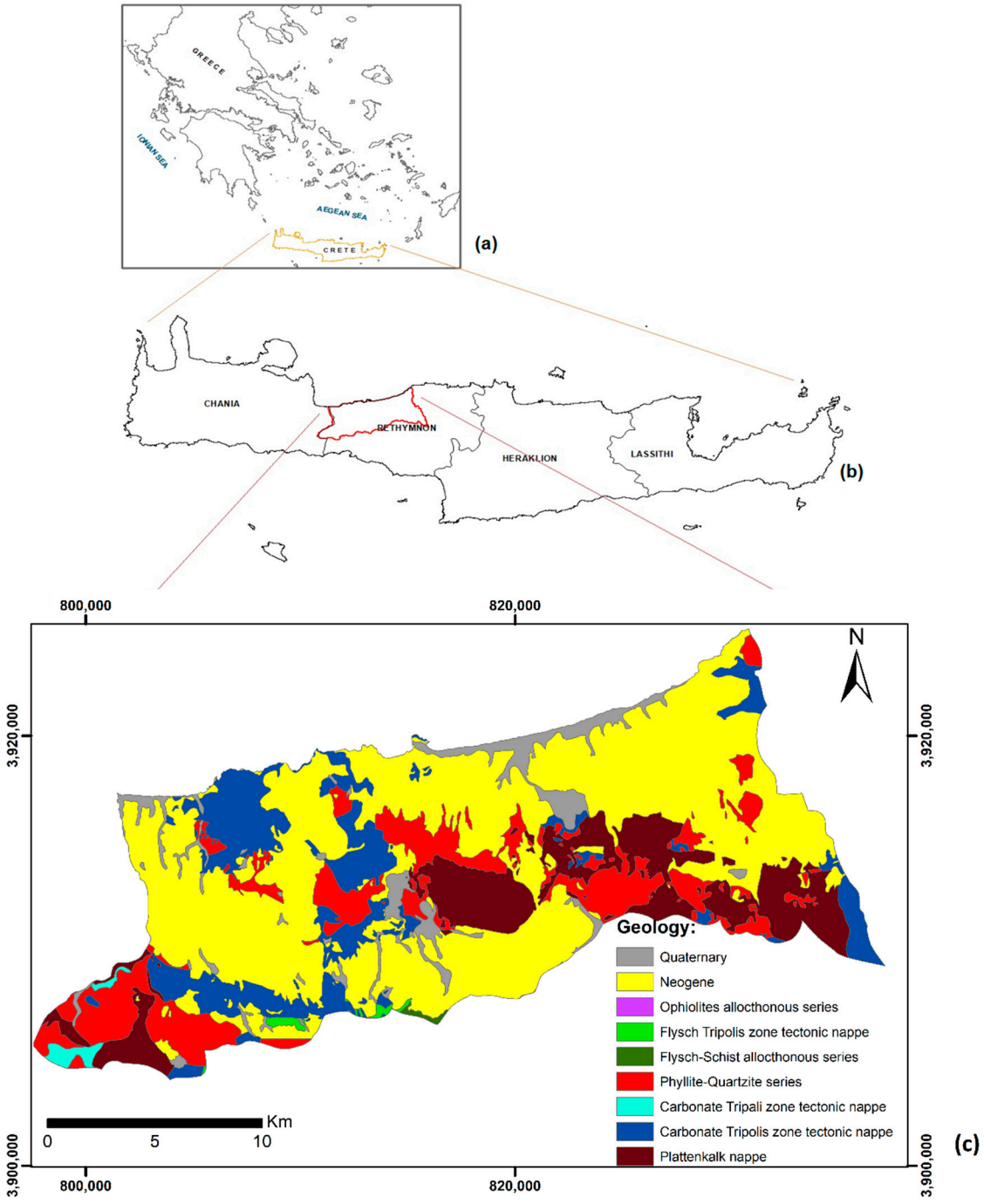

Figure 1. The area of interest (AOI) with: (**a**) location of Crete Island in Greece; (**b**) location of the municipality of Rethymnon in Crete; (**c**) geological map of the municipality of Rethymnon.

3. Methodology

There were three methodological phases in this study. The first phase consisted of the determination of the conditioning natural and anthropogenic factors associated with the occurrence of rainfall-triggered landslides. The second phase was the creation of an inventory of the rainfall-triggered landslides that occurred during the heavy rainstorms of February 2019. The third phase involved the creation of a hazard map on the basis of analyzing the spatial association between the landslide inventory and selected conditioning factors.

3.1. Determination of Conditioning Factors

Various natural factors can highlight specific climatic, morphological and lithological characteristics that can interact with each other and, under specific conditions, lead to landslide triggering. In this study, the triggering factor of rainfall, as well as the causal factors of slope gradient, landforms, rock strength and hydrolithology were considered. Anthropogenic factors can also play an important role in the increase in slope instability [27]. In this line, the factors of land use, agricultural terracing, and proximity to roads were also considered.

To determine the above factors, archived spatial datasets were acquired and processed in a GIS environment to produce raster data layers (grids) with 20 m × 20 m pixels (Table 1). The discrete classified factors such as landforms, rock strength, hydrolithology, land use, and agricultural terracing were handled in their original scale, so as to not alter the information in their data layers. The continuous numerical factors such as rainfall, slope gradient, and proximity to the road network were manually classified based on their presented values.

Table 1. Descriptive information of the spatial datasets used in this study.

Datasets	Data Source	Description
Planetscope images	Planet Lab	Multi-spectral satellite images with 3 m pixels
ALOS-PALSAR DEM	Alaska Satellite Facility (ASF) Distributed Active Archive Center (DAAC)	Digital Elevation Model (DEM) with 12.5 m spatial resolution
Geological formations	Digital Archive Library of "GeoSat ReSeArch Lab of IMS-FORTH"	Geological formations based on digitization of 1:50,000 maps (1971) of "Institute of Geology and Mineral Exploration (IGME)".
Hydrolithological formations	Digital Archive Library of "GeoSat ReSeArch Lab of IMS-FORTH"	Hydrolithological formations based on categorization of 1:50,000 maps (1971) of "Institute of Geology and Mineral Exploration (IGME)".
"CORINE" land use/cover types	Copernicus Land Monitoring Service	An inventory of land use/cover in 44 classes, which was categorized to 6 classes (urban zones, agriculture land, vegetation, dense vegetation, sparse vegetation, and water bodies).
Rainfall	Center for Hydrometeorology and Remote Sensing (CHRS), University of California	Rainfall/precipitation estimation from remotely sensed imagery using an artificial neural network cloud classification System (PERSIANN-CCS), 4 km × 4 km spatial resolution.
Road network	OpenStreeMap (OSM)	Highways, major and minor road axes.
Agricultural terraces	Google Earth (GE) platform	Identification and digitization of agricultural terraces.

3.1.1. Rainfall

Rainfall is a major triggering factor in landslide phenomena [28]. In this study, the real-time global high-resolution (4 × 4 km) satellite rainfall/precipitation product PERSIAN-CCS was used. It is based on the categorization of cloud-patch features according to cloud height, areal extent and variability of texture estimated by the satellite imagery [29]. The major advantage of PERSIAN-CCS, compared to common constant threshold approaches, is the use of a variable threshold cloud segmentation algorithm to separate individual cloud patches and categorize them with regard to their texture, geometry, cloud top height and dynamic evolution [29]. The available timesteps are hourly, 3-hourly, 6-hourly, daily, monthly and yearly.

The rainfall data highlighted several trends through the years for the study area. From a yearly perspective, after fluctuations between 2003 and 2017, a remarkable increase in overall rainfall amount was generally observed from 2017 to mid-2019 over the municipality of Rethymnon (Figure 2). Specifically in mid-2019, this amount was the highest recorded since 2003.

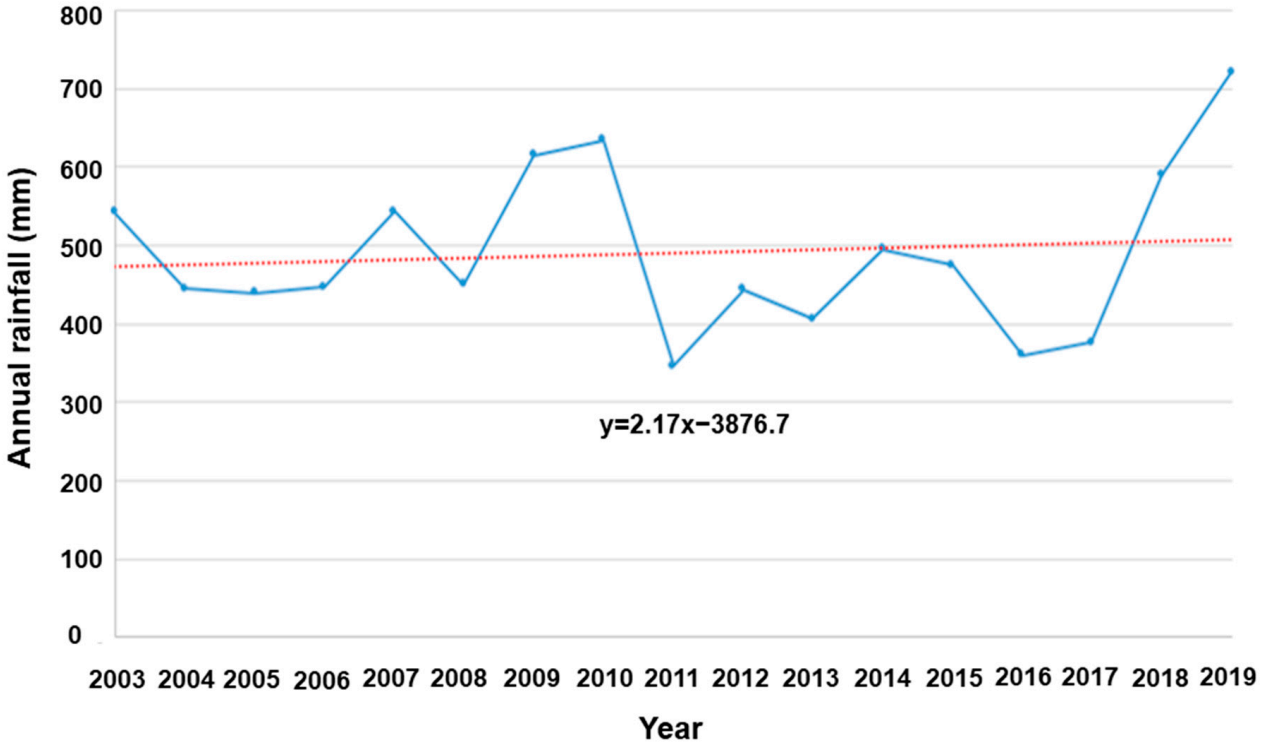

Figure 2. Annual rainfall (mm) for the municipality of Rethymnon during the period 2003 to 2019.

From a monthly perspective, a mean rainfall of approximately 147 mm fell in February 2019 (Table 2). During this month, two severe rainstorm events named as "Hioni" (13–17 February) and "Okeanis" (24–26 February) took place in Crete, causing extensive flooding and landslides in residential and rural areas across the island, with the recorded rainfall amount in many regions being three to four times higher than the mean rainfall of western Crete [3]. Among the severely affected areas was the municipality of Rethymnon, with the damage from both events on its infrastructure (damage to the road network and constructions) and agricultural land (destruction of crops) estimated to have cost in the order of EUR ~50,000,000 [30]. In general, the short-term occurrence of a few days between the two storm events of "Hioni" and "Okeanis" can be considered as a continuous storm event, with most of the domino-effect landslides taking place during the "Okeanis" event. Considering the triggering of landslides during these events as a result of period-specific impact, the significant rainfall amounts over the study area for the period from September 2018 to February 2019 were taken into account (Table 2). The cumulative rainfall for this

period was used to represent the triggering factor of rainfall, with the higher values being mainly observed in the north-western section of the study area (Figure 3). These data were derived from the resampling of the PERSIANN-CCS data grids, and separated into five classes: (i) <450 mm, (ii) 450–500 mm, (iii) 500–550 mm, (iv) 550–600 mm, and (v) >600 mm.

Table 2. Monthly mean rainfall (mm) for the municipality of Rethymnon, during the period between September 2018 and February 2019.

City	Source	Month	Monthly Mean Rainfall (mm)
Rethymno	PERSIANN-CCS	18 September	42.8
Rethymno	PERSIANN-CCS	18 October	29.9
Rethymno	PERSIANN-CCS	18 November	96.1
Rethymno	PERSIANN-CCS	18 December	56.3
Rethymno	PERSIANN-CCS	19 January	171.5
Rethymno	PERSIANN-CCS	19 Febuary	147.3

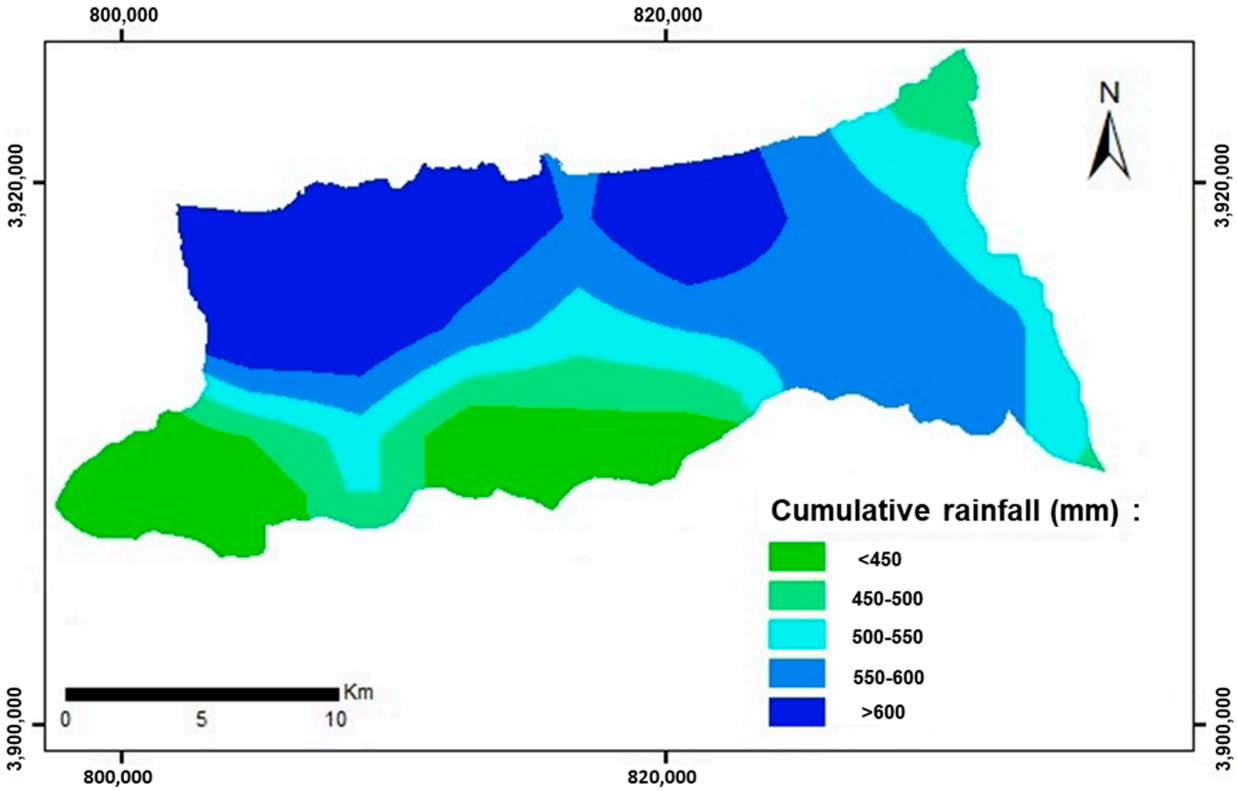

Figure 3. The spatial distribution of cumulative rainfall (mm) across the municipality of Rethymnon, during the period between September 2018 and February 2019.

3.1.2. Slope Gradient

The slope gradient highlights maximum slope steepness according to the change in elevation between each pixel and its neighbors [31]. In areas with steep slopes, periods of intense rainfall can trigger surface run-off, slope instability and landslides [28,32]. Extracted as ALOS-Palsar DEM derivative, slope gradient was separated into five classes: (i) slightly gentle, (ii) gentle, (iii) moderate, (iv) steep, and (v) extremely steep (Figure 4a). Slope gradient was calculated in degrees using free open-source software QGIS (Version 3.24-Tisler).

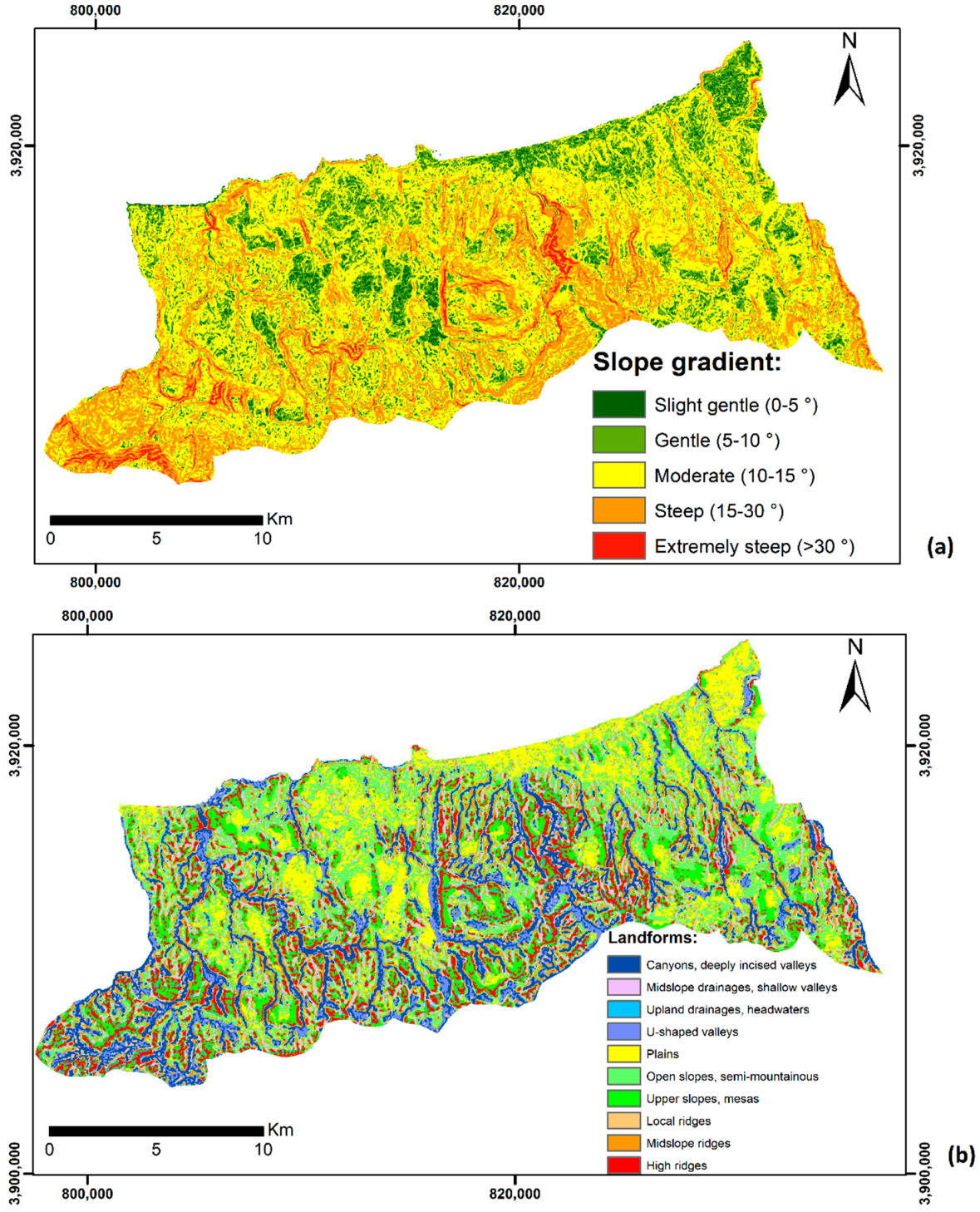

Figure 4. *Cont.*

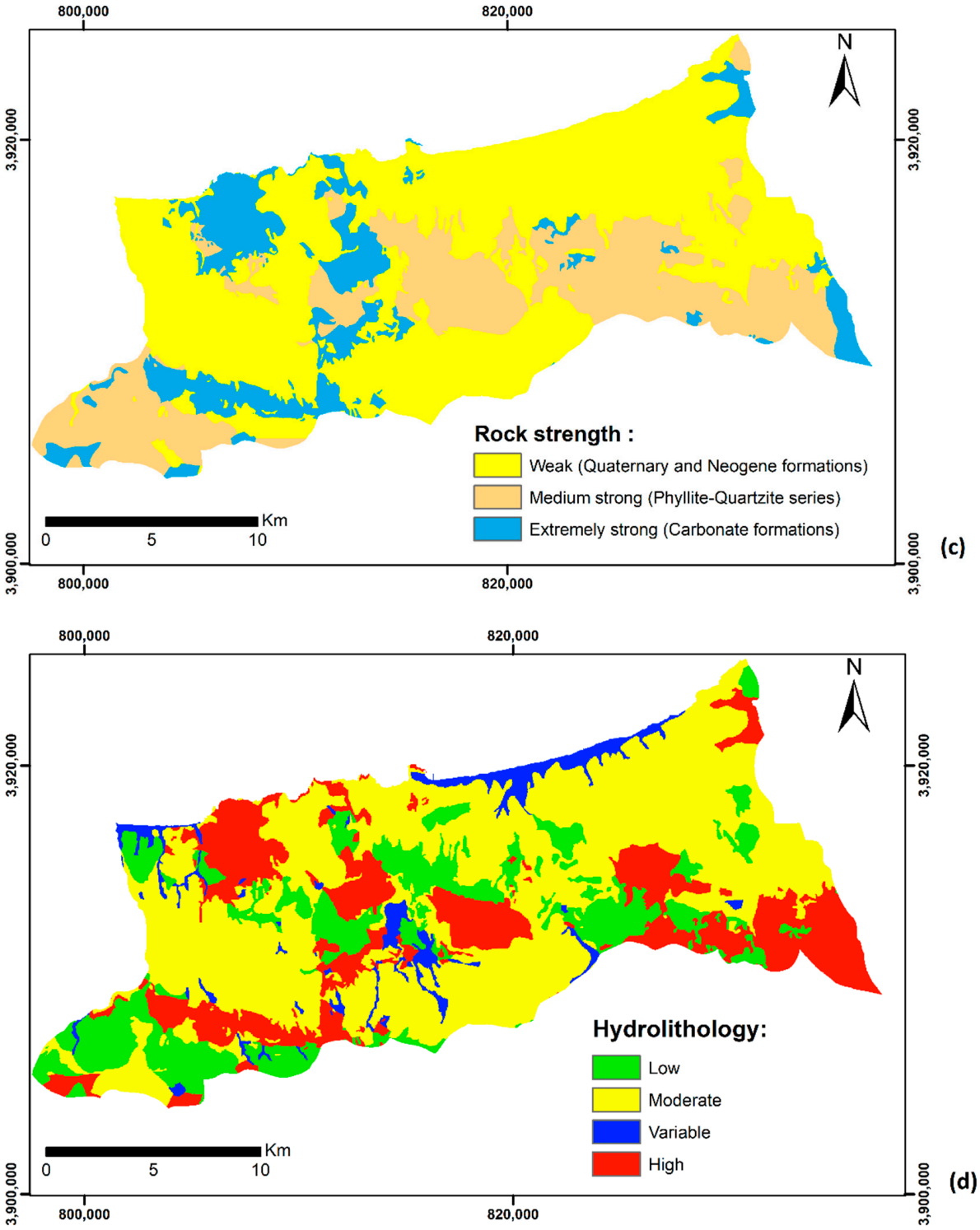

Figure 4. Natural conditioning factors: (**a**) slope gradient; (**b**) landforms; (**c**) rock strength; (**d**) hydrolithology.

3.1.3. Landforms

The landform classification was based on Topographic Position Index (TPI) analysis, extracted as ALOS-Palsar DEM derivatives. Usually, two neighborhood sizes are combined to offer detailed geomorphological information through the discrimination of complex landscape features, as a single neighborhood size provides less information about the general shape of the landscape [33]. In this study, the two combined neighborhood sizes

in each case were based on the study of Argyriou et al. [34] who, after combining various neighborhood sizes, found the combination of 300 m and 1000 m for characterizing regions of Crete as the most reliable system. The TPI-based landform classification produced ten landform types: (i) canyons, (ii) mid-slope drainages, (iii) upland drainages, (iv) U-shaped valleys, (v) plains, (vi) open slopes, (vii) upper slopes, (viii) local ridges, (ix) mid-slope ridges, and (x) high ridges (Figure 4b).

3.1.4. Rock Strength

The factor of rock strength was extracted by grouping the geological formations of the study area (Figure 1c) according to the Geological Strength Index (GSI) [35]. This resulted to three classes: (i) weak, (ii) medium strong, and (iii) extremely strong (Figure 4c). Weak, unconsolidated lithologies result in formations being more vulnerable to landsliding in relation to strong lithologies, which are more resistant [6,36].

3.1.5. Hydrolithology

Hydrolithology highlights the rainfall-related permeability levels of lithological formations as extracted by grouping the geological formations of the study area (Figure 1c). The derived hydrolithological classes are: (i) low; (ii) moderate; (iii) high; and (iv) variable (Figure 4d).

3.1.6. Land Use

Land-use types were derived by the open source "CORINE" 2018 dataset, with 44 initial classes being grouped into the following nine: (i) urban zones, (ii) arable land, (iii) permanent crops (vineyards and olive groves), (iv) pastures, (v) heterogeneous agricultural areas, (vi) forests, (vii) scrub vegetation, (viii) no vegetation, and (ix) water bodies (Figure 5a).

3.1.7. Agricultural Terracing

Agricultural terraces over weak sedimentary formations associated with heavy rainfall can contribute to slope instability [9]. Agricultural terraces that do not have proper support walls can lead to soil saturation under heavy rain conditions, resulting in soil instability and subsequent soil erosion [9]. In this study, the terraces of the study area were digitized over multi-temporal images provided by the free open-source Google Earth (GE) platform (Figure 5b).

3.1.8. Proximity to Road Network

Road networks—especially in a mountainous terrain such as this study area—can be a major factor for landsliding, since the man-made cutting of slopes for roads can cause slope instability when related to weak rock strength and heavy rainfall periods [6,27]. Highway information, as well as that of major and minor roads of the study area, was based on the datasets of the open-source OpenStreetMap platform. As proximity to the road network can affect landslide occurrence, the creation of buffer zones along the road network was accomplished for the following nine classes: (i) 0–10 m, (ii) 10–25 m, (iii) 25–50 m, (iv) 50–75 m, (v) 75–100 m, (vi) 100–150, (vii) 150–200 m, (viii) 200–300 m, and (ix) >300 m (Figure 5c).

3.2. Detection of Landslide Occurrence

There are various RS-based techniques of processing satellite imagery that can be applied to extract useful environmental and natural hazard information. Considering that landslides contribute to landscape alteration, the technique of pixel-based change detection in satellite images can be used to semi-automatically detect these changes. PlanetScope satellite imagery provides daily illustrations of the Earth's surface at a high spatial resolution (3 m). This daily frequent pass coverage of the satellite sensor offers the opportunity to assess the damage of a hazardous event upon the first cloud-free available satellite images pre- and post-event. Thus, by comparing the images before and after the period of a heavy

rainfall event, it will be possible to detect and capture any soil displacement triggered by the specific event.

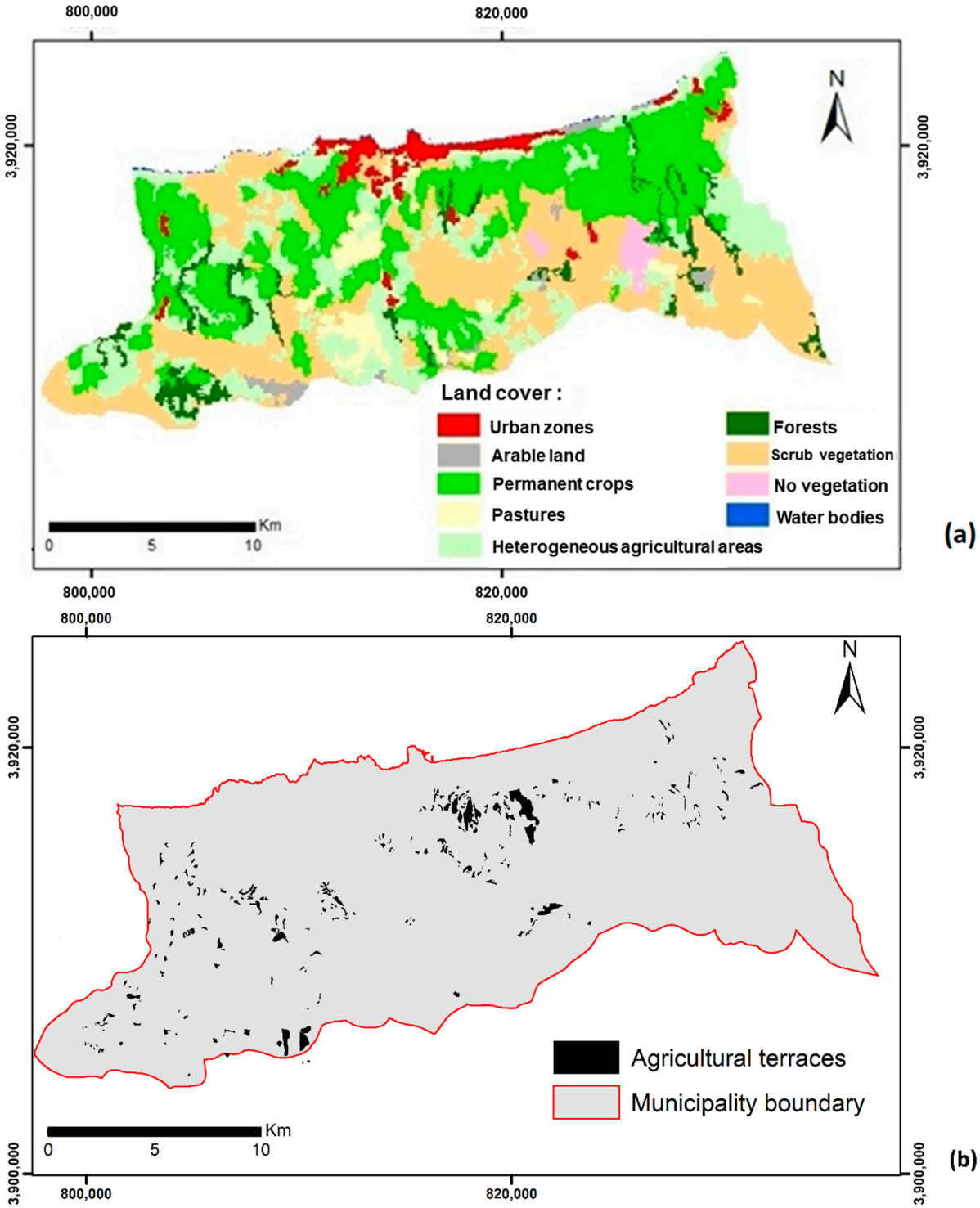

Figure 5. *Cont.*

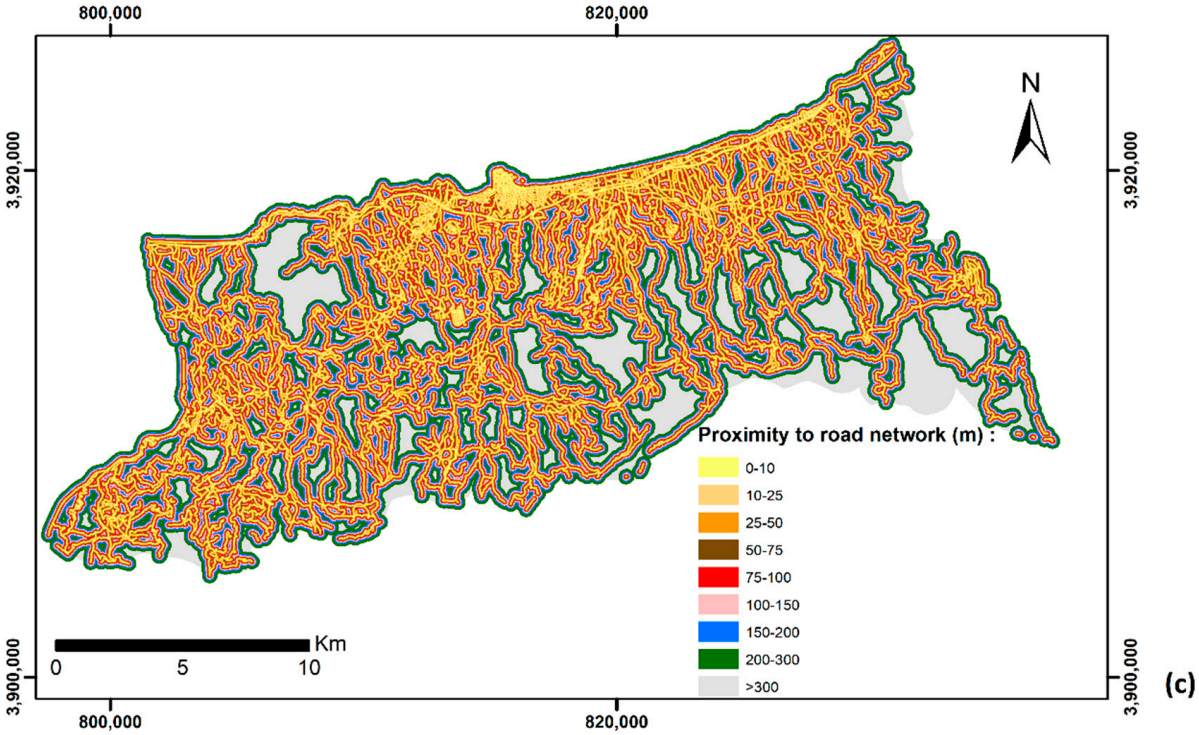

Figure 5. Anthropogenic conditioning factors: (**a**) land use; (**b**) agricultural terracing; (**c**) proximity to road network.

In this study, the temporal comparison between pre- and post-event PlanetScope multispectral satellite images was accomplished through a specific algorithm (Zonal Change Detection Express) in ERDAS Imagine-2015 (Hexagon, AL, USA) processing software. In particular, within the algorithm, the difference in spectral values of the images before and after the rainstorm event (Figure 6) was analyzed to produce a map presenting the possibility of changes between the two temporal images. Moreover, this technique calculated the change percentage for specified survey zones/polygons using boundary values for the change map. A probability value of 0.95 was defined for this study, indicating the portion of each polygon to which the probability of change was greater than 95%. A square grid (3×3 m) was used to define the polygon, which was extended to the entire study area (by overlaying the image difference of the two temporal images).

3.3. Landslide Hazard Mapping

In terms of landslide hazard and susceptibility assessment, areas with conditions similar to those of the affected areas of Crete studied here are likely to experience landslides in future extreme rainfall events [37]. The statistics-based determination of the effects of conditioning factors on past landslide occurrence in the affected areas represents a statistical analysis model for estimating the relative probability of landslides in unaffected areas. Depending on the examination of factors individually or cumulatively, these models can be either bivariate [38–40] or multivariate [41–43]. In particular, bivariate models include the association of each individual factor with a landslide inventory, and the estimation of weight values based on the landslide densities for its classes [43]. All the factors were sampled in the multivariate models, and the presence or absence of landslide was determined for each of the sampling units. Then, weight values were calculated for the factors via statistical means.

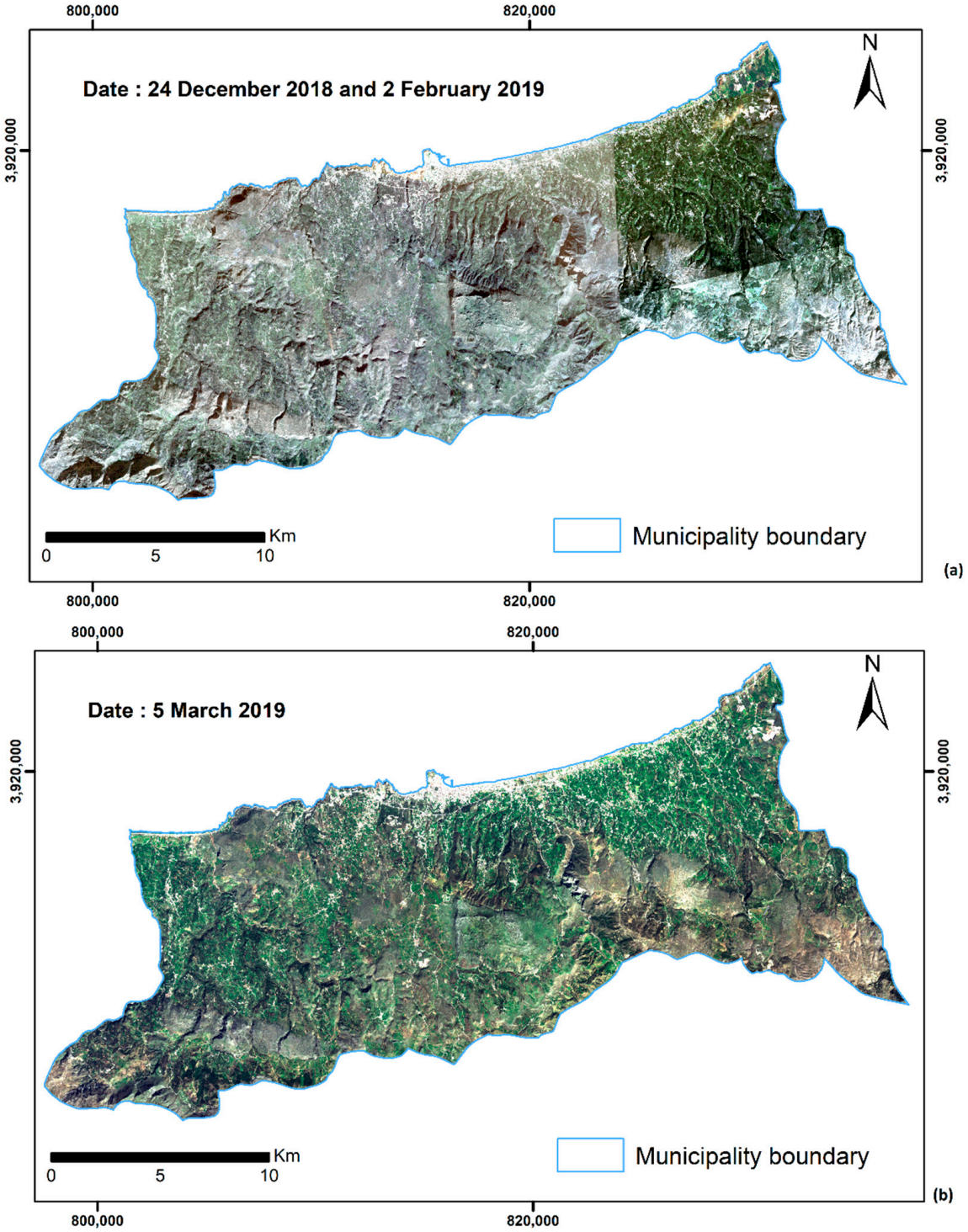

Figure 6. PlanetScope satellite images for the municipality of Rethymnon: (**a**) pre-event image; (**b**) post-event image.

3.3.1. Weight of Evidence

Weight of evidence (WoE) is a statistical bivariate model with the basic principles of the prior (or unconditional) and posterior (or conditional) probabilities, based on Bayes'

theorem [44]. Prior probability (P) of landslide occurrence is determined by the total amount of landslides (L) occurred in the past, within the total extent of a given region (T):

$$P\{L\} = \frac{N\{L\}}{N\{T\}} \tag{1}$$

The prior probability can be modified by including determinants that influence it. These determinants are considered as "evidences". When the "evidence" is integrated into the calculation of probability, it is addressed as posterior, expressing the probability that a landslide will occur under either the presence (B) or the absence ($\overline{B}$) of an "evidence" [45]:

$$P\{L|B\} = \frac{P\{L \cap B\}}{P\{B\}} = P\{L\}\frac{P\{B|L\}}{P\{B\}} \tag{2}$$

$$P\{L|\overline{B}\} = \frac{P\{L \cap \overline{B}\}}{P\{\overline{B}\}} = P\{L\}\frac{P\{\overline{B}|L\}}{P\{\overline{B}\}} \tag{3}$$

Considering each class of a geo-environmental factor as an "evidence", a pair of weights is calculated according to the aforementioned probabilities. These weights indicate the significance of the presence (W^+) or absence (W^-) of the specific class of landslide occurrence, and are derived from the following natural logarithms [46]:

$$W^+ = \ln\frac{P\{B|L\}}{P\{B|\overline{L}\}} = \ln\left(\frac{\frac{A_1}{A_1+A_2}}{\frac{A_3}{A_3+A_4}}\right) \tag{4}$$

$$W^- = \ln\frac{P\{\overline{B}|L\}}{P\{\overline{B}|\overline{L}\}} = \ln\left(\frac{\frac{A_2}{A_1+A_2}}{\frac{A_4}{A_3+A_4}}\right) \tag{5}$$

where A_1 is the amount of landslides in a specific factor class, A_2 is the amount of landslides in the rest of the factor classes, A_3 is the not-landslide-affected area of the specific factor class, and A_4 is the not-landslide-affected area of the rest of the factor classes. The difference between the two weights, known as contrast (C), quantitatively determines whether there is an impact/how significant the impact is for each factor class on the occurrence of past landslides:

$$C = W^+ - W^- \tag{6}$$

A positive C value indicates a spatial association, whereas a negative value indicates that a spatial association is lacking [47]. An overall landslide hazard (LH) value can be estimated by the summation of the contrast values of examined factors:

$$LH = \sum_{i=1}^{n} C_{i,j} \tag{7}$$

where $C_{i,j}$ is the contrast value for the class j of the factor i, and n is the total number of the factors.

3.3.2. Validation

Validation is a crucial step in landslide hazard modeling because it can provide information about the accuracy and prediction ability of a model. A standard validation method, known as receiver operating characteristics (ROC) analysis, was used for this purpose. In general, ROC analysis depends on two fundamental concepts: sensitivity and specificity. They are derived by the Equations below [48]:

$$Sensitivity = \frac{n(TP)}{n(TP) + n(FN)} \tag{8}$$

$$Specificity = \frac{n(TN)}{n(TN) + n(FP)} \quad (9)$$

where *n(TP)* and *n(FP)* are the amounts of true and false positive predictions, respectively. A true positive is a prediction of landslide activity at a location where landsliding has actually occurred, while a false positive is a prediction of landslide at a location where the landsliding has not actually occurred [49]. Conversely, *n(TN)* and *n(FN)* are the amounts of true and false negative predictions, respectively. A curve is designed in an ROC graph, with sensitivity representing the y-axis and the difference of 1−specificity representing the x-axis [48]. The value of area under curve (AUC) reveals the prediction ability of a model. Ranging from 0.5 to 1.0, the higher this value the better the model's predictivity.

4. Results

The overall results of the methodological framework acknowledged within this study are described below.

Regarding the RS-based landslide detection, the differences in spectral values of images before and after the rainstorm events with the change percentage for specified survey zones/polygons using boundary values for the change map are shown in Figure 7, indicating the portion of each polygon of which the probability of change was greater than 95%. By the specific change-detection technique, changes in pixels that correspond to agricultural activities (e.g., land plowing) or topography-based shadow effects (due to different sun angles when the satellite images were taken) were also detected. In order to overcome these limitations, the change detection results were qualitatively evaluated by means of the visual interpretation of the temporal satellite images and subsequent field surveys (Figures 8 and 9). In this way, the changes associated exclusively with landslides were accurately identified and validated. The identified landslides were related to shallow debris flows and earth slides (Figures 8 and 9), with the majority of them being less than 0.005 km^2.

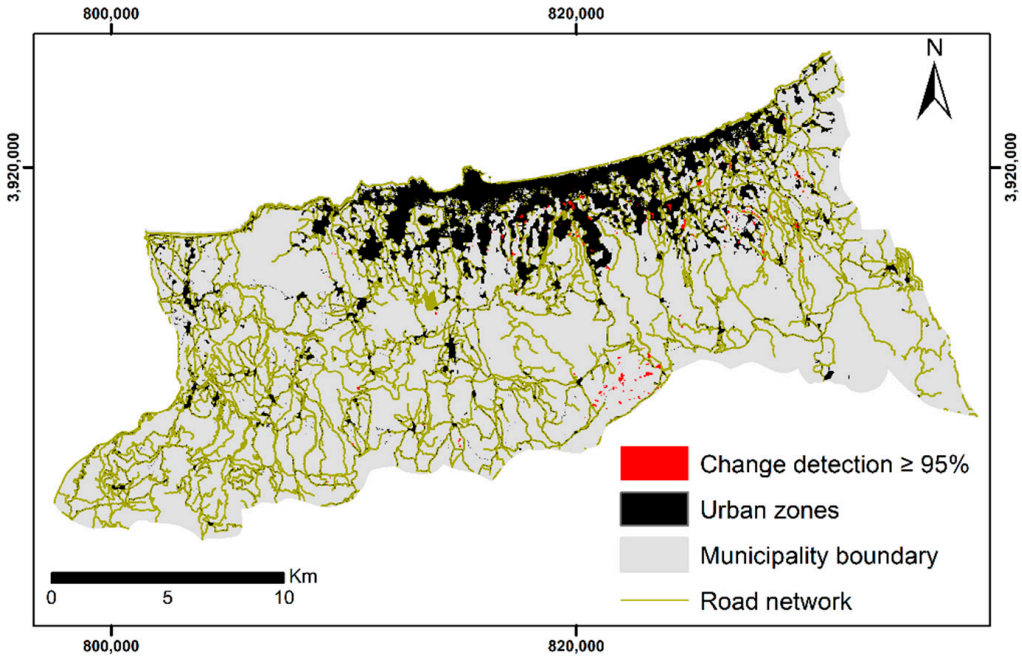

Figure 7. Change detection result, with spectral change percentage greater than 95% between the same pixels of pre- and post-event PlanetScope satellite images.

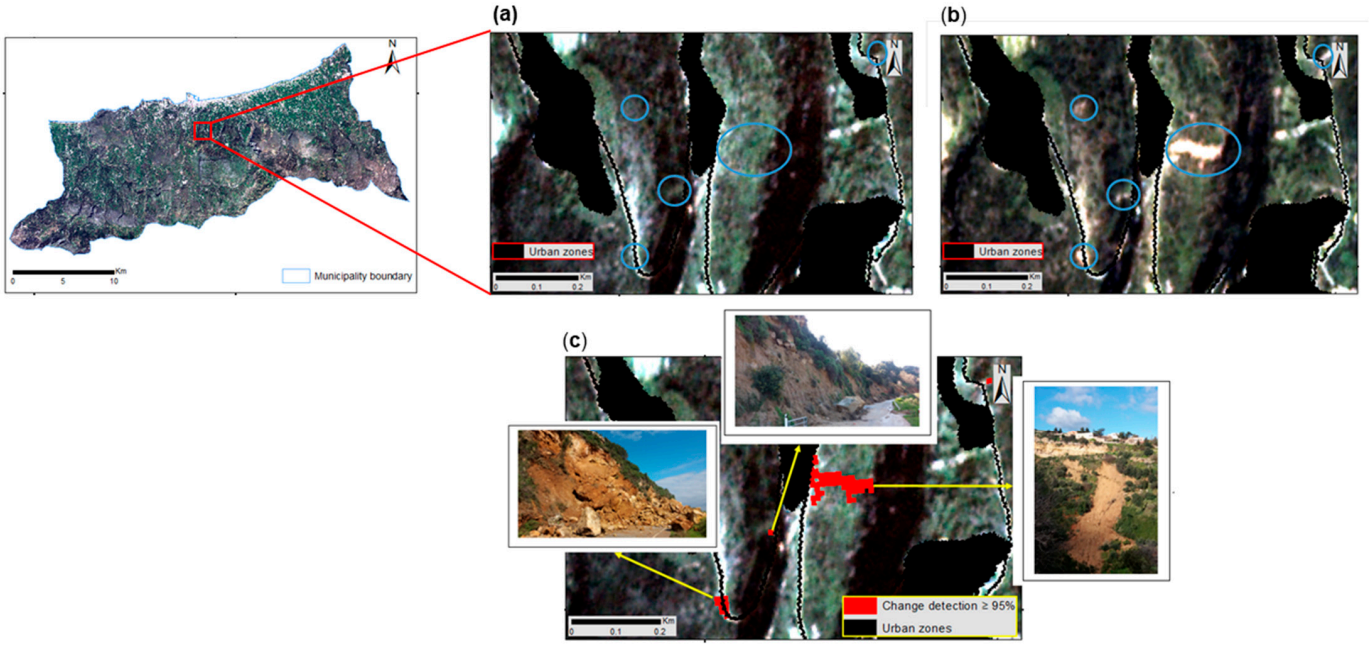

Figure 8. PlanetScope satellite images for a part of the Municipality of Rethymnon: (**a**) pre-event image, (**b**) post-event image. At (**c**) the change percentage greater than 95% on each pixel is highlighted in zones (red color). Blue circles in pre-event and post-event images highlight the changes in pixels corresponding to landslides. The black color mask corresponds to urban zones.

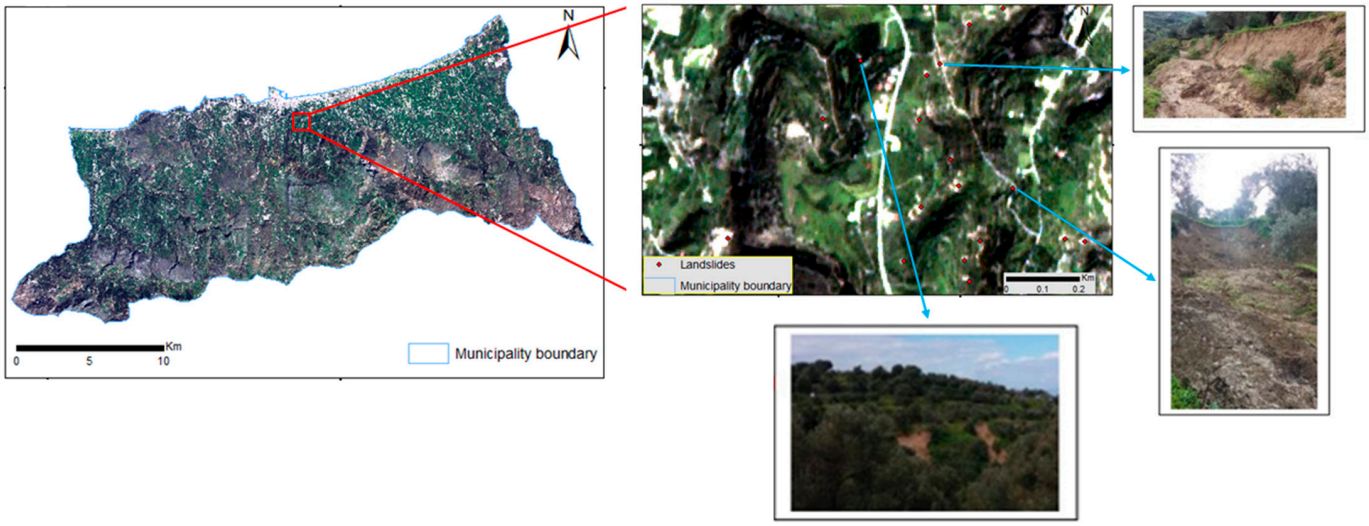

Figure 9. PlanetScope image of part of the study area (left image) showing landslide locations in yellow points. The arrows point to photographs of the specific landslides, taken during field surveys.

The final result of the overall landslide detection procedure was an inventory map. Landslide inventory maps may be prepared by different techniques based on the analysis scale. Smaller-scale maps may present only landslide locations, whereas larger-scale maps may identify the definite areas of landslides [50]. Hence, considering the small analysis scale, as well as the quite small coverage area of the majority of identified landslides, the inventory map of this study was selected to present the features of the locations of landslides triggered by the "Hioni" and "Okeanis" rainstorm events. In total, 826 landslide locations for the municipality of Rethymnon were included (Figure 10).

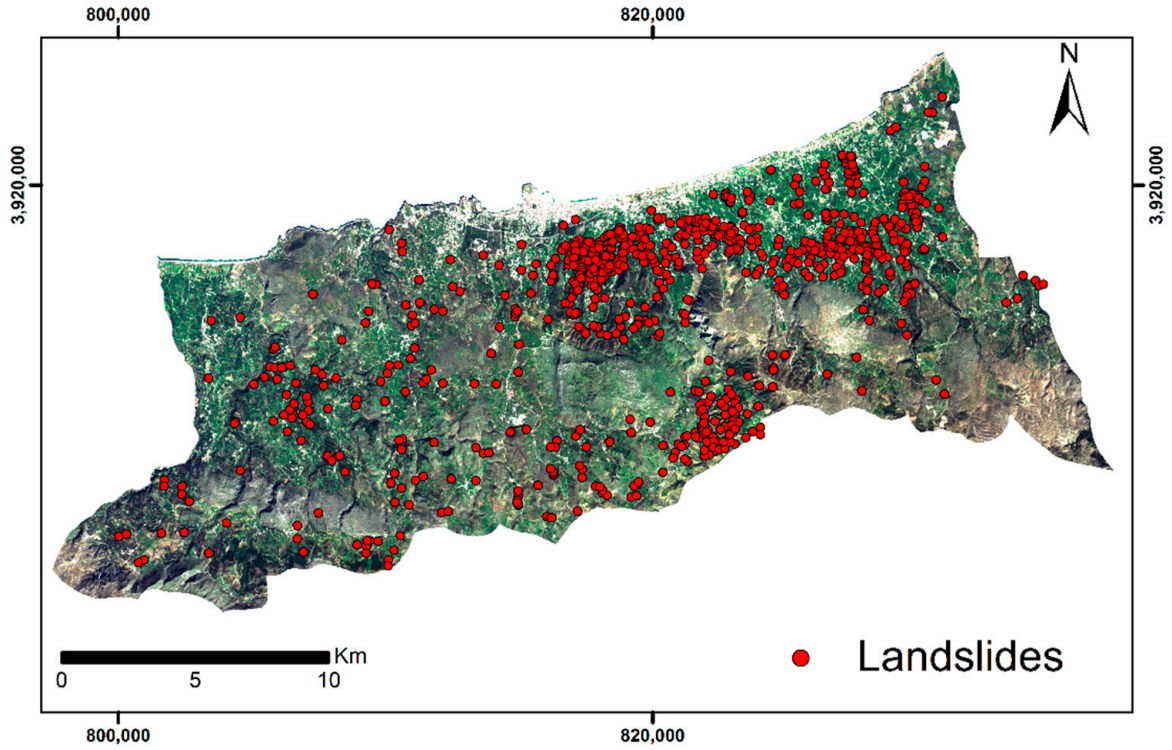

Figure 10. Landslide inventory map with 826 landslide locations detected.

In terms of GIS-based landslide hazard assessment, the WoE model was applied in this study. The sampling of the dataset from the landslide inventory map was initially conducted. The sampling process included the separation of the dataset into two parts, one for the training of the model and one for the validation of its produced result. Therefore, among the total landslide inventory data (826 points), 80% (659 points) was randomly selected to create the training dataset, and the remaining 20% (167 points) composed the validation dataset. By overlaying the training dataset on each of the factors, the WoE statistics for all factor classes were estimated based on Equations (4)–(6). In order to interpret the importance of each factor, the range and the standard deviation of their *C* values were also calculated. WoE statistics for all factor classes and the range and the standard deviation of their *C* values are shown in Table 3. After the assignment of estimated *C* values as weights to the relative factor classes, the summation of the weighted factors (Equation (7)) was implemented to produce the landslide hazard map. The map was eventually classified into three classes ("Low", "Moderate", and "High" hazard) based on the "Natural Breaks" classification method (Figure 11).

Table 3. Weights and contrast values for the factor classes, and contrast-based ranges and standard deviations for the factors.

Factors and Their Classes	W^+	W^-	C	C_{RANGE}	C_{SD}
Rainfall (mm)				3.85	1.58
[1] <450	−2.48	0.07	−2.55		
[2] 450−500	−0.29	0.03	−0.32		
[3] 500−550	−0.24	0.04	−0.28		
[4] 550−600	0.20	−1.10	1.30		
[5] >600	0.21	−1.09	1.30		

Table 3. *Cont.*

Factors and Their Classes	W^+	W^-	C	C_{RANGE}	C_{SD}
Slope gradient				1.22	0.46
[1] Slightly gentle	−0.53	0.02	−0.54		
[2] Gentle	−0.59	0.09	−0.68		
[3] Moderate	−0.04	0.04	−0.08		
[4] Steeep	0.38	−0.16	0.54		
[5] Extremely steep	0.20	−0.01	0.21		
Rock strength				3.01	1.53
[1] Weak	0.41	−1.29	1.70		
[2] Medium strong	−0.04	0.22	−0.26		
[3] Extremely strong	−1.18	0.13	−1.31		
Hydrolithology				2.85	1.17
[1] Low	−0.37	0.07	−0.44		
[2] Moderate	0.38	−0.86	1.24		
[3] Variable	−0.10	0.005	−0.10		
[4] High	−1.39	0.22	−1.61		
Landforms				1.62	0.57
[1] Canyons	0.51	−0.09	0.60		
[2] Mid-slope drainages	0.66	−0.08	0.74		
[3] Upland drainages	−0.01	0.00	−0.01		
[4] U-shaped valleys	−0.08	0.01	−0.08		
[5] Plains	−0.80	0.08	−0.88		
[6] Open slopes	0.02	−0.01	0.03		
[7] Upper slopes	−0.80	0.06	−0.86		
[8] Local ridges	−0.39	0.00	−0.40		
[9] Mid-slope ridges	0.25	−0.03	0.28		
[10] High ridges	−0.60	0.05	−0.65		
Land use				3.81	1.09
[1] Urban zones	−2.49	0.03	−2.52		
[2] Arable land	−0.11	0.002	−0.11		
[3] Permanent crops	0.71	−0.57	1.28		
[4] Pastures	−0.62	0.02	−0.64		
[5] Heterogeneous agricultural areas	−0.46	0.10	−0.56		
[6] Forests	0.61	−0.04	0.65		
[7] Scrub vegetation	−0.89	0.25	−1.13		
[8] No vegetation	NA	0.01	−0.01		
[9] Water bodies	NA	0.002	−0.002		
Agricultural terracing				1.32	0.93
[1] No	0.58	−0.08	0.66		
[2] Yes	−0.08	0.58	−0.66		
Proximity to road network (m)				1.04	0.31
[1] 0-10	−0.07	0.01	−0.07		
[2] 10−25	0.05	−0.01	0.05		
[3] 25−50	0.33	−0.07	0.39		
[4] 50−75	0.14	−0.02	0.16		
[5] 75−100	0.13	−0.01	0.14		
[6] 100−150	0.07	−0.01	0.08		
[7] 150−200	−0.08	0.01	−0.08		
[8] 200−300	−0.34	0.03	−0.38		
[9] >300	−0.59	0.06	−0.65		

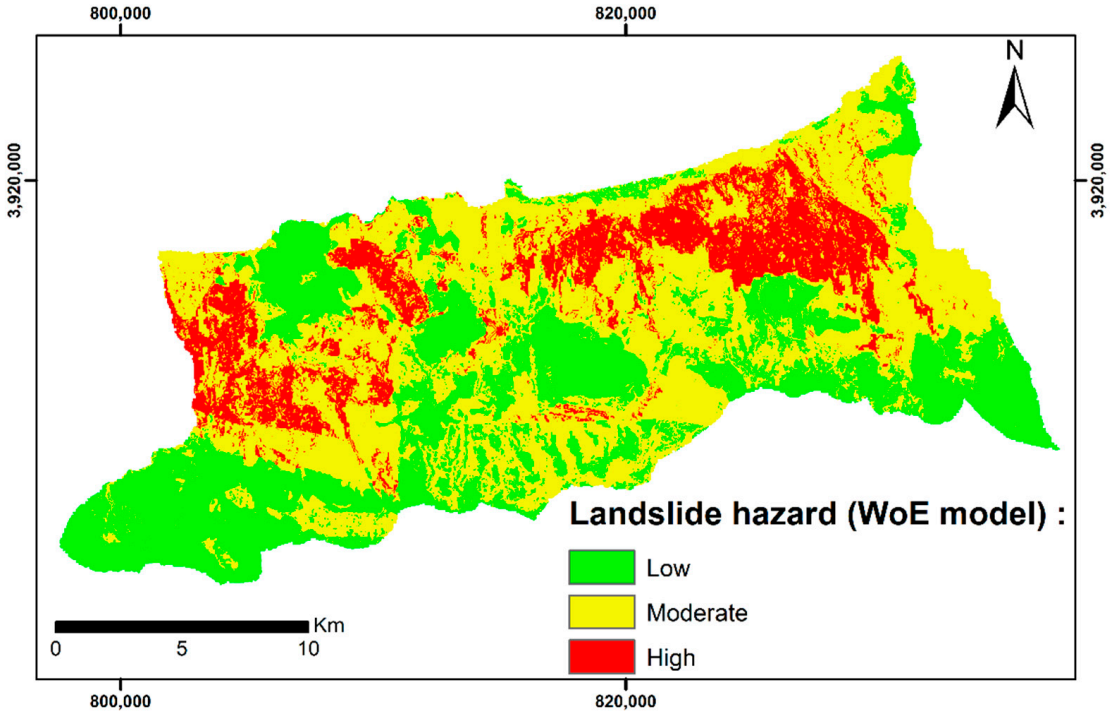

Figure 11. Landslide hazard map produced by WoE model.

For the validation of the model's resultant map, the ROC analysis was applied by using the "independent" landslide validation dataset. Moreover, an equal number of data from the not-landslide-affected area were randomly selected. The ROC curve was drawn and the relative metrics are shown in Figure 12 and Table 4.

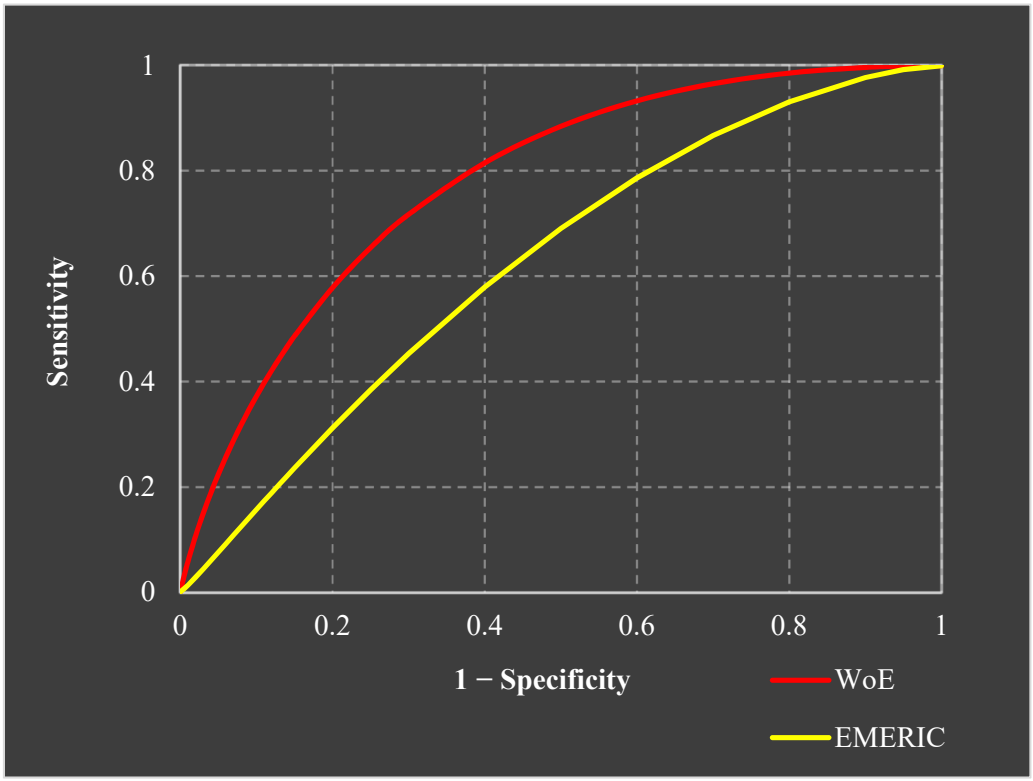

Figure 12. ROC curves.

Table 4. ROC analysis metrics.

Metrics	WoE	EMERIC
Number of cases	334	334
Number correct	219	197
Positive cases missed	9	29
Negative cases missed	106	108
Sensitivity (%)	94.6	82.6
Specificity (%)	36.5	35.3
AUC	0.78	0.63

5. Discussion

In this study, a geoinformatics-based methodological framework was developed for analyzing rainfall-triggered landslides in terms of the synergistic use of RS and GIS technologies. Generally, the advantage of RS technology to cover large regions at high frequency has enabled relevant approaches to become popular for detecting the spatial distribution of landslides at different spatio-temporal scales [51,52]. To corroborate the effectiveness and applicability of RS, a pixel-based change detection approach was applied on pre- and post-event high-resolution satellite images, for semi-automatically detecting landslides that occurred as a result of two catastrophic rainstorm events on Crete Island. Considering the multispectral differences between the images, this approach facilitates a rapid and reasonably accurate landslide detection method over large areas, where pre-event and post-event satellite imagery are available. Nevertheless, this requires the definition of appropriate threshold values which are decided on a case-by-case basis [53]. For the current case study, the validation conducted by field surveys indicated that the chosen RS-based approach was able to recognize rainfall-triggered landslides with a relatively high accuracy, and PlanetScope imagery constituted a good data source because of its advantages of multispectral high-resolution images and daily revisits.

Several natural and anthropogenic factors were GIS-analyzed, searching for a better understanding of their impact on the occurrence of rainfall-triggered landslides. Since no official guidelines have been provided by the scientific community for their selection, the characteristics of the study area, the scale of analysis and data availability, as well as relevant literature [6,27,28,54] were taken into account for this study.

The impact of each factor was quantitatively expressed by class-level estimations of the WoE model. The model was based on the observed landslide densities to expose the spatial correlation between the phenomenon's occurrence and factors in the study area. Its basic advantage was that missing factor data and under-sampled landslide data as inputs did not significantly affect its results [55]. The assumption of conditional independence, i.e., the fact that the different factors were independent with respect to the probability of the occurrence of a landslide, can be mentioned as its main disadvantage [56]. Statistical models such WoE are generally considered the most appropriate method for landslide hazard mapping at regional scales because they are objective, reproducible and easily updatable [37]. However, under the need for independence of the statistical distribution of the data and an analysis being quite accurate with a small amount of data, other quantitative models such as machine learning models are commonly recommended. Thus, the scale of analysis and the properties of collected data were the major criteria which the selection of the applied statistical model was based on.

The results of the WoE model are summarized in Table 3. The factor classes with the highest *C* values were found to be "weak" (*C* = 1.70) for rock strength, "550 to 600 mm" and "over 600 mm" (*C* = 1.30) for rainfall, "permanent crops" (*C* = 1.28) for land use, "moderate" (*C* = 1.24) for hydrolithology, "mid-slope drainages" (*C* = 0.74) for landforms, "no" (*C* = 0.66) for agricultural terracing, "steep" (*C* = 0.54) for slope gradient, and "25 to 50 m" (*C* = 0.39) for proximity to road network. Hence, for the municipality of Rethymnon, areas with mainly steep terrains being very close to roads, covered by hydrolithologically weak formations exploited for permanent cropping (vineyards or olive groves) without the

presence of terraces, and affected by very high amounts of rainfall, were more prone in landsliding during or after the "Hioni" and "Okeanis" rainstorms. Furthermore, according to the estimated standard deviation statistics, the highest value was presented by the rainfall factor (C_{SD} = 1.58), followed by the rock strength factor (C_{SD} = 1.53). Proximity to the road network was the factor with the lowest value (C_{SD} = 0.31). This finding, represented by the WoE-based ranking of rainfall as the most influential factor, can confirm the "nature" of the examined landslides as rainfall-triggered events.

Based on the above results of the WoE model, a landslide hazard map was produced (Figure 11). By visualizing the spatial distribution of the classified hazard ("Low", "Moderate", and "High"), this map divided the study area into zones with regard to their probability for landsliding in the future under the influence of a potential rainstorm similar (in terms of rainfall amount and/or intensity) to those of February 2019. As shown in Figure 11, the "High" hazard was mainly concentrated in the western and north-eastern parts of the municipality of Rethymnon. Notably, 16% of the study area was covered by the corresponding hazard class (Figure 13). The coverage percentages for the other two classes, "Low" and "Moderate", were 35% and 49%, respectively. Despite the comparatively smaller coverage extent, the majority of landslides (over 50%) were correlated to the zone of "High" hazard (Figure 13). At the same time, fewer landslides (below 40% and 10%, respectively) occurred within the more extensive zones of "Moderate" and "Low" hazard.

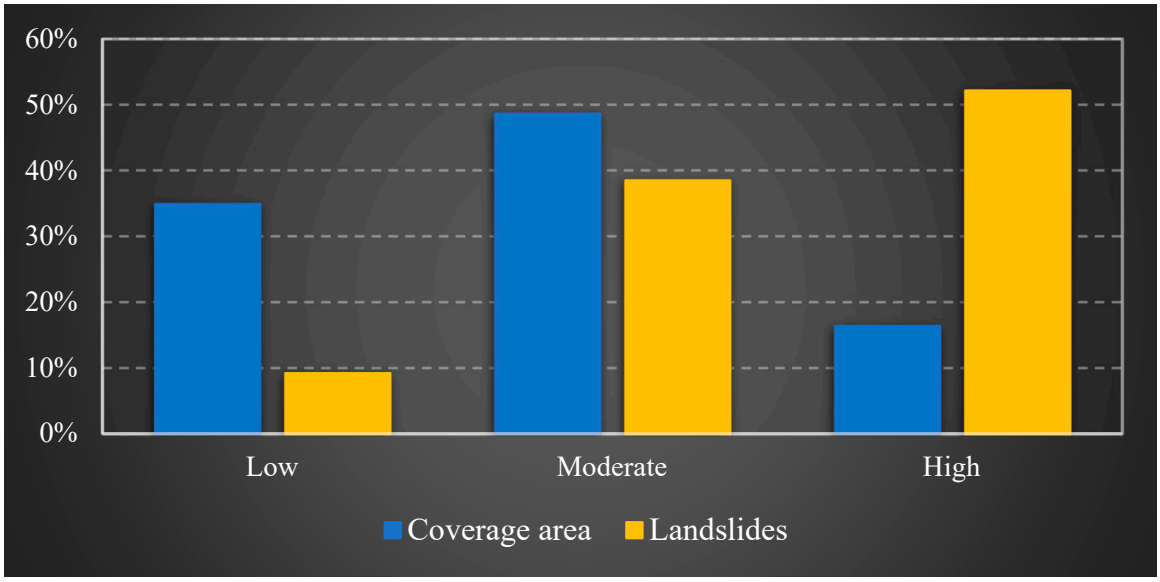

Figure 13. Coverage area and landslide percentages for the hazard classes.

The reliability of the produced hazard map, and thus the prediction ability of the WoE model, was evaluated by means of validation using a landslide dataset not originally included in its training process. The results of ROC analysis are presented in Figure 12 and Table 4. The estimated AUC value of 0.78, as well as the values of 94.6% and 36.5% for the sensitivity and specificity, respectively, demonstrated a very promising prediction ability for the applied model. The resultant AUC value seems to be in agreement with other landslide studies applying WoE for different regions [47,57–59]. Furthermore, among statistical analysis models, WoE has been proved to give better validation results compared to other bivariate [60–62] or multivariate [63,64] models for landslide hazard and susceptibility assessments.

The validation results for another landslide hazard map of the study area, produced under the EC-funded "EMERIC" project of 2000–2006 [15], are also presented in Figure 12 and Table 4. For the creation of this map (Figure 14), five conditioning factors (geology, hydrolithology, slope gradient, rainfall and distance from faults) were analyzed by an expert-based weighting model. Considering their AUC values, where a higher sensitivity

is linked to truer positive (correct) predictions and a higher specificity results in fewer false positive (incorrect) predictions, the WoE quantitative model gives much better results than the EMERIC's qualitative model. So, it is clear that zones being presented as moderate ones in the EMERIC's map seem to be of higher hazard in the WoE model's map, on the basis of acknowledging factors that the EMERIC did not consider in its analysis, such as agriculture terracing and unprecedented rainfall. Especially, the agriculture terracing was one of the main factors to acknowledge in this study, as the fieldwork visits proved that the lack of defensive walls led to slope instability, with the landslide occurrence in upper terraces drifting to lower elevated terraces as well. This could result in forthcoming soil erosion in the future in these areas, and local authorities need to take action to support defensive wall practices in these agricultural terraces.

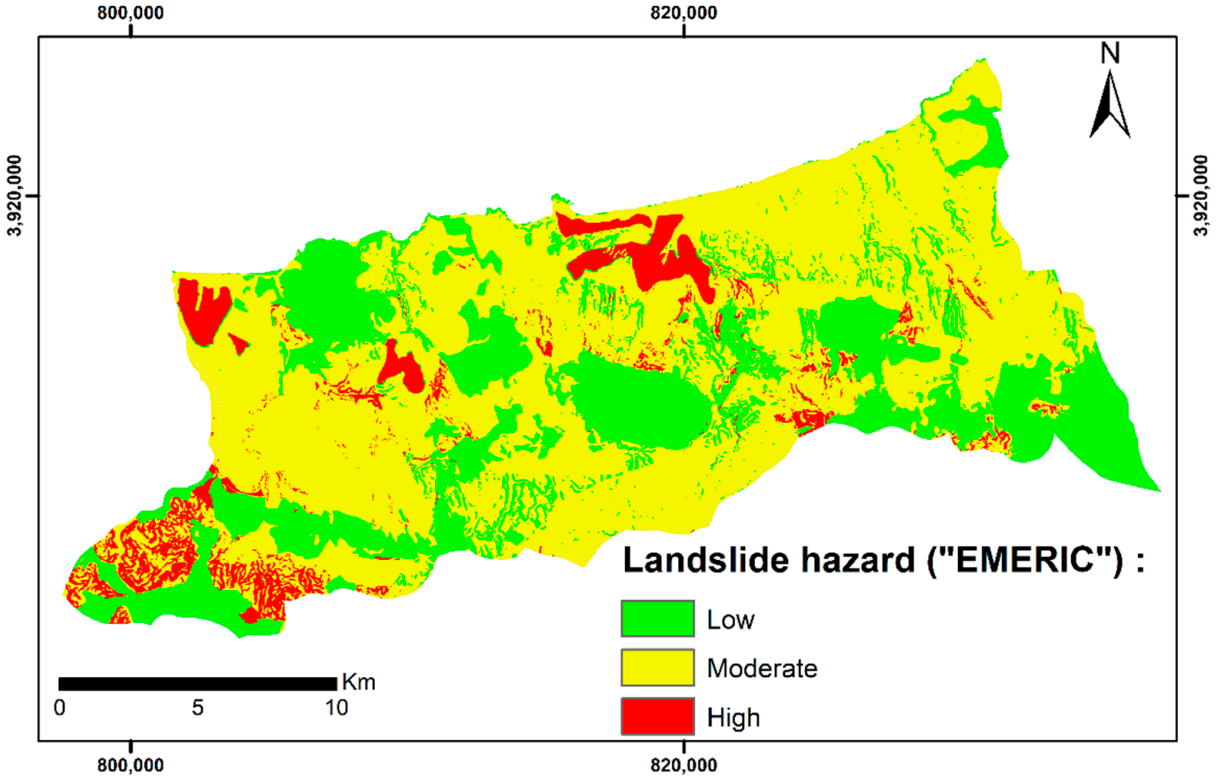

Figure 14. Landslide hazard map produced under "EMERIC" project.

The limitations of the study, herein, are mainly focused on the sampling procedure to determine the training and validation datasets which can influence the efficiency of the adopted model to retrieve the final landslide hazard map. A respectively balanced and sufficient amount of datasets should be distributed on the acknowledged training samples and the validation ones. In terms of the conditioning factors, the spatial resolution and the derived threshold values during their classification method can produce slight mismatches between the detected landslide locations and the factor datasets. Even if the main regional trends of the highlighted landslide hazard zones remain, further statistical investigation of these parameters is needed to increase the precision of the model. In addition, the change detection procedure of the temporal satellite images highlights the issue of changes in pixels corresponding to agricultural activities (e.g., land plowing) or topography-based shadow effects (due to different sun angles when the satellite images were taken) which need to be qualitatively evaluated by means of visual interpretation of the different satellite images and subsequent field surveys. So, further investigation to enrich the change detection algorithm with parameters that can detect these effects needs to be carried out, and the algorithm must follow an automated procedure to avoid means of visual interpretation.

It is worth mentioning that, in this study, important analysis parameters such as the applied approaches (pixel-based change detection rather than, e.g., object-based) and models (statistical WoE rather than, e.g., machine learning), the number, type and preprocessing of conditioning factors, the size of training and validation datasets, as well as the classification of resultant hazard map, were based on objective criteria. Considering the data-driven "nature" of the analysis, the examination of alternative choices for these parameters could lead to different results.

Geological processes such as landslides seriously threaten the safety of human life, property, ecological resources and the environment. Their accurate prediction and effective control can reduce the cost of disaster management by providing recommendations to avoid human injury and the unnecessary waste of material and financial resources, and realize long-term sustainable development. By promoting the advancement of geoinformatic technologies for landslide prevention and control, the findings of this study can ensure the sustainable development of the ecological environment and, to some degree, contribute to the sustainable development of the regional economy. Another aspect of this study is the value of the adopted methodological framework towards sustainability and effective long-term land use in similar Mediterranean regions. As in this study, other studies have used similar tools, such as freely available or low-cost satellite datasets via the use of Free Open-Source Software (FOSS), such as QGIS, for geospatial data analysis and mapping, focusing on sustainable geoinformatics [65] and the reduction in digital data poverty [66]. The presented methodology removes a major cost barrier and enables sustainable geoinformatics [65]. It can also be used to guide land-use management in the context of climate change and probable increased occurrences of similar landslide-triggering storm events, in conjunction with other relevant studies that have taken place around Mediterranean environments [67–69].

6. Conclusions

For the island of Crete, with geological and morpho-climatic settings that are typical of the Mediterranean region, the occurrence of severe rainstorms—with a potential increase in severity and frequency due to climate change—acting as a triggering mechanism for landslides is a common phenomenon. Hence, the acquisition of knowledge about the impact of conditioning factors on the occurrence of rainfall-triggered landslides, as well as about the parts of island that are more likely to be affected by them in the future, can be considered as crucial needs. A multidisciplinary geoinformatics-based methodological framework, using diverse factors associated with landslide activity, was examined and evaluated in this study. These factors were considered with regard to their inter-relationships and their significance in the occurrence of "domino-effect" landslide phenomena as a result of the extreme "Hioni" and "Oceanis" rainstorms. This resulted in numerous landslide events, with their locations being detected by an RS-based technique and plotted on an inventory map. A landslide hazard map was then created for the study area by applying a data-driven quantitative model (WoE). The model was based on the landslide inventory and its relation to environmental and anthropogenic factors.

In general, this research can be beneficial to evaluate the significance of conditioning factors for landslide activity in the Mediterranean region, and help other studies focusing on the assessment of landslide hazards and susceptibility. Due to its confirmed reliability, the hazard map produced by the WoE model provides a basis for the assessment and management of landslide phenomena in Crete. In particular, this map can assist local authorities and decision makers to identify areas and infrastructures subject to damage by future rainfall-induced landslides, and take measures and actions for landslide prevention or mitigation in the case of extreme rainfall events to follow in the future. Moreover, by using the same map, suitable locations for future construction activities can be targeted to avoid their exposure to landslide phenomena.

This study highlights the benefits of geoinformatic technologies to develop a methodological framework to better understand conditioning factors and their threshold limits

for causing landslide activity in a region. A landslide early-warning system can thus be provided. Recommended further research includes: (i) further testing the WoE model's predictivity by correlating its hazard map with landslides triggered by future extreme rainstorm events; and (ii) comparison with other statistical (both bivariate and multivariate) methods and advanced machine learning models.

Author Contributions: Conceptualization, A.V.A.; methodology, A.V.A. and C.P.; software, A.V.A. and C.P.; validation, A.V.A. and C.P.; formal analysis, A.V.A. and C.P.; data curation, A.V.A. and C.P.; writing—original draft preparation, A.V.A., C.P., R.M.T. and N.P.; writing—review and editing, A.V.A., C.P., R.M.T. and N.P.; visualization, A.V.A. and C.P.; supervision, R.M.T. and N.P. All authors have read and agreed to the published version of the manuscript.

Funding: This research received no external funding.

Institutional Review Board Statement: Not applicable.

Informed Consent Statement: Not applicable.

Data Availability Statement: Not applicable.

Acknowledgments: The authors extremely appreciate the significant contributions of the journal's editor and reviewers to the handling and revision of this article. Special thanks to Planet Labs and Planet's Education and Research (E&R) Program for the PlanetScope imageries availability.

Conflicts of Interest: The authors declare no conflict of interest.

References

1. Froude, M.J.; Petley, D.N. Global fatal landslide occurrence from 2004 to 2016. *Nat. Hazards Earth Syst. Sci.* **2018**, *18*, 2161–2181. [CrossRef]
2. Bathrellos, G.D.; Kalivas, D.P.; Skilodimou, H.D. Landslide Susceptibility Assessment Mapping: A Case Study in Central Greece. In *Remote Sensing of Hydrometeorological Hazards*, 1st ed.; Petropoulos, G.P., Islam, T., Eds.; CRC Press: Boca Raton, FL, USA, 2017; Chapter 18.
3. Psomiadis, E.; Papazachariou, A.; Soulis, K.X.; Alexiou, D.-S.; Charalampopoulos, I. Landslide Mapping and Susceptibility Assessment Using Geospatial Analysis and Earth Observation Data. *Land* **2020**, *9*, 133. [CrossRef]
4. Sabatakakis, N.; Koukis, G.; Mourtas, D. Composite landslides induced by heavy rainfalls in suburban areas: City of Patras and surrounding area, western Greece. *Landslides* **2005**, *2*, 202–211. [CrossRef]
5. Kouli, M.; Loupasakis, C.; Soupios, P.; Rozos, D.; Vallianatos, F. Landslide susceptibility mapping by comparing WLC and WofE multi-criteria methods in the West Crete Island, Greece. *Environ. Earth Sci.* **2014**, *72*, 5197–5219. [CrossRef]
6. Skilodimou, H.D.; Bathrellos, G.D.; Koskeridou, E.; Soukis, K.; Rozos, D. Physical and Anthropogenic Factors Related to Landslide Activity in the Northern Peloponnese, Greece. *Land* **2018**, *7*, 85. [CrossRef]
7. Farahmand, A.; AhaKouchak, A. A satellite-based global landslide model. *Nat. Hazards Earth Syst. Sci.* **2013**, *13*, 1259–1267. [CrossRef]
8. Kirschbaum, D.; Stanley, T. Satellite-based assessment of rainfall-triggered landslide hazard for situational awareness. *Earth's Future* **2018**, *6*, 505–523. [CrossRef]
9. Moreno-de-las-Heras, M.; Lindenberger, F.; Latron, J.; Lana-Renault, N.; Llorens, P.; Arnáez, J.; Romero-Díaz, A.; Gallart, F. Hydro-geomorphological consequences of the abandonment of agricultural terraces in the Mediterranean region: Key controlling factors and landscape stability patterns. *Geomorphology* **2019**, *333*, 73–91. [CrossRef]
10. Grove, A.T.; Rackham, O. *The Nature of Mediterranean Europe: An Ecological History*; Yale University Press: London, UK, 2003.
11. Arnáez, J.; Lana-Renault, N.; Lasanta, T.; Ruiz-Flaño, P.; Castroviejo, J.J. Effects of farming terraces on hydrological and geomorphological processes. A review. *Catena* **2015**, *128*, 122–134. [CrossRef]
12. Debussche, M.; Lepart, J.; Dervieux, A. Mediterranean landscape changes: Evidence from old postcards. *Glob. Ecol. Biogeogr.* **1999**, *8*, 3–15. [CrossRef]
13. Lourenço, L.; Nunes, A.N.; Bento-Gonçalves, A.; Vieira, A. Environmental Concerns of Portuguese Mountains: A Case Study in the Central Mountains. In *Mountains: Geology, Topography and Environmental Concerns*; Gonçalves, A.J.B., Vieira, A.A.B., Eds.; Nova Science Publishers: New York, NY, USA, 2014; Chapter 6; pp. 195–211.
14. Brunetti, M.T.; Melillo, M.; Gariano, S.L.; Ciabatta, L.; Brocca, L.; Amarnath, G.; Peruccacci, S. Satellite rainfall products outperform ground observations for landslide prediction in India. *Hydrol. Earth Syst. Sci.* **2021**, *25*, 3267–3279. [CrossRef]
15. Sarris, A.; Karakoudis, S.; Bidaki, X.; Soupios, P. Study of the morphological attributes of Crete through the use of remote sensing techniques. *IASME Trans.* **2005**, *2*, 1043–1051.
16. Kelletat, D. Perspectives in coastal geomorphology of western Crete, Greece. *Z. Geomorphol. Suppl.* **1996**, *102*, 1–19.

17. Shaw, B.; Ambraseys, N.N.; England, P.C.; Floyd, M.A.; Gorman, G.J.; Higham, T.F.G.; Jackson, J.A.; Nocquet, J.-M.; Pain, C.C.; Piggott, M.D. Eastern Mediterranean tectonics and tsunami hazard inferred from the AD 365 earthquake. *Nat. Geosci.* **2008**, *1*, 268–276. [CrossRef]
18. Stiros, S. Late Holocene relative sea level changes is SW Crete evidence of an unusual earthquake cycle. *Ann. Geophys.* **1996**, *3*, 677–687. [CrossRef]
19. Fassoulas, C.; Rahl, J.; Ague, J.; Henderson, K. Patterns and conditions of deformation in the Plattenkalk nappe, Crete, Greece: A preliminary study. *Bull. Geol. Soc. Greece* **2004**, *36*, 1626–1635. [CrossRef]
20. Argyriou, A.V.; Teeuw, R.M.; Rust, D.; Sarris, A. GIS multi-criteria decision analysis for assessment and mapping of neotectonic landscape deformation: A case study from Crete. *Geomorphology* **2016**, *253*, 262–274. [CrossRef]
21. ELSTAT. 2011 Population and Housing Census. Available online: https://www.statistics.gr/ (accessed on 20 March 2021).
22. Christaras, B. Landslides in iliolitic and marly formations. Examples from nort-western Greece. *Eng. Geol.* **1997**, *47*, 57–69. [CrossRef]
23. Miščević, P.; Števanić, D.D.; Štambuk-Cvitanović, N. Slope instability mechanisms in dipping conglomerates over weathered marls: Bol landslide, Croatia. *Environ. Geol.* **2009**, *56*, 1417–1426. [CrossRef]
24. Markopoulos, T.; Rotondo, P.; Chrysafaki, G.; Mousourakis, A. Evaluation of mudstone formations from Crete and their suitability for rammed earth and adobe production. *Proc. Sci. Conf. SGEM* **2008**, *1*, 659–673.
25. Papanikolaou, D.; Vassilakis, E. Thrust faults and extensional detachment faults in Cretan tectono-stratigraphy: Implications for Middle Miocene extension. *Tectonophysics* **2010**, *488*, 233–247. [CrossRef]
26. Parikh, S.J.; James, B.R. Soil: The Foundation of Agriculture. *Nat. Educ. Knowl.* **2012**, *3*, 2.
27. Bathrellos, G.D.; Kalivas, D.P.; Skilodimou, H.D. GIS-based landslide susceptibility mapping models applied to natural and urban planning in Trikala, Central Greece. *Estud. Geol.* **2009**, *65*, 49–65. [CrossRef]
28. Donati, L.; Turrini, M.C. An objective method to rank the importance of the factors predisposing to landslides with the GIS methodology: Application to an area of the Apennines (Valnerina; Perugia, Italy). *Eng. Geol.* **2002**, *63*, 277–289. [CrossRef]
29. Nguyen, P.; Shearer, E.J.; Tran, H.; Ombadi, M.; Hayatbini, N.; Palacios, T.; Huynh, P.; Updegraff, G.; Hsu, K.; Kuligowski, B.; et al. The CHRS Data Portal, an easily accessible public repository for PERSIANN global satellite precipitation data. *Nat. Sci. Data* **2019**, *6*, 180296. [CrossRef]
30. Region of Crete. Press Releases. Available online: https://www.crete.gov.gr/press-releases/ (accessed on 15 September 2021).
31. Dunn, M.; Hickey, R. The effect of slope algorithms on slope estimates within a GIS. *Cartography* **1998**, *27*, 9–15. [CrossRef]
32. Chudý, F.; Slámová, M.; Tomaštík, J.; Prokešová, R.; Mokroš, M. Identification of Micro-Scale Landforms of Landslides Using Precise Digital Elevation Models. *Geosciences* **2019**, *9*, 117. [CrossRef]
33. Tagil, S.; Jenness, J. GIS-Based Automated Landform Classification and Topographic, Landcover and Geologic Attributes of Landforms Around the Yazoren Polje, Turkey. *J. Appl. Sci.* **2008**, *8*, 910–921. [CrossRef]
34. Argyriou, A.V.; Teeuw, R.M.; Sarris, A. GIS-based landform classification of Bronze Age archaeological sites on Crete Island. *PLoS ONE* **2017**, *12*, e0170727. [CrossRef]
35. Marinos, P.; Hoek, E. GSI: A geologically friendly tool for rock mass strength estimation. In Proceedings of the GeoEng2000 at the International Conference on Geotechnical and Geological Engineering, Melbourne, Australia, 19–24 November 2000; Technomic Publishing: Lancaster, PA, USA, 2000; pp. 1422–1442.
36. Foster, C.; Jenkins, G.O.; Gibson, A.D. *Landslides and Mass Movements Processes and Their Distribution in the York District (Sheet 63)*; Open Report; British Geological Survey: Nottingham, UK, 2007; pp. 1–49.
37. He, Y.; Beighley, R.E. GIS-based regional landslide susceptibility mapping: A case study in southern California. *Earth Surf. Process. Landf.* **2008**, *33*, 380–393. [CrossRef]
38. Kayastha, P. Landslide susceptibility mapping and factor effect analysis using frequency ratio in a catchment scale: A case study from Garuwa sub-basin, East Nepal. *Arab. J. Geosci.* **2015**, *8*, 8601–8613. [CrossRef]
39. Chen, W.; Xie, X.; Peng, J.; Shahabi, H.; Hongd, H.; Tien Bui, D.; Duan, Z.; Li, S.; Zhud, A.-X. GIS-based landslide susceptibility evaluation using a novel hybrid integration approach of bivariate statistical based random forest method. *Catena* **2018**, *164*, 135–149. [CrossRef]
40. Wu, H.; Song, T. An evaluation of landslide susceptibility using probability statistic modeling and GIS's spatial clustering analysis. *Hum. Ecol. Risk Assess. Int. J.* **2018**, *24*, 1952–1968. [CrossRef]
41. Reichenbach, P.; Busca, C.; Mondini, A.C.; Rossi, M. The Influence of Land Use Change on Landslide Susceptibility Zonation: The Briga Catchment Test Site (Messina, Italy). *Environ. Manag.* **2014**, *54*, 1372–1384. [CrossRef]
42. Dagdelenler, G.; Nefeslioglu, H.A.; Gokceoglu, C. Modification of seed cell sampling strategy for landslide susceptibility mapping: An application from the Eastern part of the Gallipoli Peninsula (Canakkale, Turkey). *Bull. Eng. Geol. Environ.* **2016**, *75*, 575–590. [CrossRef]
43. Polykretis, C.; Grillakis, M.G.; Argyriou, A.V.; Papadopoulos, N.; Alexakis, D.D. Integrating multivariate (GeoDetector) and bivariate (IV) statistics for hybrid landslide susceptibility modeling: A case of the vicinity of Pinios artificial lake, Ilia, Greece. *Land* **2021**, *10*, 973. [CrossRef]
44. Bonham-Carter, G.F. *Geographic Information Systems for Geoscientists: Modeling with GIS*; Pergamon Press: Ottawa, ON, Canada, 1994.

45. Poonam, C.; Rana, N.; Champati Ray, P.K.; Bisht, P.; Bagri, D.S.; Wasson, R.J.; Sundriyal, Y. Identification of landslide-prone zones in the geomorphically and climatically sensitive Mandakini valley, (central Himalaya), for disaster governance using the Weights of Evidence method. *Geomorphology* **2017**, *284*, 41–52.
46. Guri, P.K.; Champati Ray, P.K.; Patel, R.C. Spatial prediction of landslide susceptibility in parts of Garhwal Himalaya, India, using the weight of evidence modelling. *Environ. Monit. Assess.* **2015**, *187*, 324. [CrossRef]
47. Kayastha, P.; Dhital, M.R.; De Smedt, F. Landslide susceptibility mapping using the weight of evidence method in the Tinau watershed, Nepal. *Nat. Hazards* **2012**, *63*, 479–498. [CrossRef]
48. Fawcett, T. An introduction to ROC analysis. *Pattern Recognit. Lett.* **2006**, *27*, 861–874. [CrossRef]
49. Akgun, A. A comparison of landslide susceptibility maps produced by logistic regression, multi-criteria decision, and likelihood ratio methods: A case study at İzmir, Turkey. *Landslides* **2012**, *9*, 93–106. [CrossRef]
50. Guzzetti, F.; Mondini, A.C.; Cardinali, M.; Fiorucci, F.; Santangelo, M.; Chang, K.T. Landslide inventorymaps: New tools for an old problem. *Earth-Sci. Rev.* **2012**, *112*, 42–66. [CrossRef]
51. Mondini, A.C.; Guzzetti, F.; Reichenbach, P.; Rossi, M.; Cardinali, M.; Ardizzone, F. Semi-automatic recognition and mapping of rainfall induced shallow landslides using optical satellite images. *Remote Sens. Environ.* **2011**, *115*, 1743–1757. [CrossRef]
52. Singh, P.; Maurya, V.; Dwivedi, R. Pixel based landslide identification using Landsat 8 and GEE. *Int. Arch. Photogramm. Remote Sens. Spat. Inf. Sci.* **2021**, *XLIII-B3-2021*, 721–726. [CrossRef]
53. Zhao, W.; Li, A.; Nan, X.; Zhang, Z.; Lei, G. Postearthquake Landslides Mapping From Landsat-8 Data for the 2015 Nepal Earthquake Using a Pixel-Based Change Detection Method. *IEEE J. Sel. Top. Appl. Earth Obs. Remote Sens.* **2017**, *10*, 1758–1768. [CrossRef]
54. Bachri, S.; Shrestha, R.P.; Yulianto, F.; Sumarmi, S.; Utomo, K.S.B.; Aldianto, Y.E. Mapping Landform and Landslide Susceptibility Using Remote Sensing, GIS and Field Observation in the Southern Cross Road, Malang Regency, East Java, Indonesia. *Geosciences* **2021**, *11*, 4. [CrossRef]
55. Regmi, N.R.; Giardino, J.R.; Vitek, J.D. Modeling susceptibility to landslides using the weight of evidence approach: Western Colorado, USA. *Geomorphology* **2010**, *115*, 172–187. [CrossRef]
56. Van Westen, C.J. The Modelling Of Landslide Hazards Using GIS. *Surv. Geophys.* **2000**, *21*, 241–255. [CrossRef]
57. Oh, H.-J.; Lee, S. Landslide susceptibility mapping on Panaon Island, Philippines using a geographic information system. *Environ. Earth Sci.* **2011**, *62*, 935–951. [CrossRef]
58. Hussin, H.Y.; Zumpano, V.; Reichenbach, P.; Sterlacchini, S.; Micu, M.; van Westen, C.; Bălteanu, D. Different landslide sampling strategies in a grid-based bi-variate statistical susceptibility model. *Geomorphology* **2016**, *253*, 508–523. [CrossRef]
59. Torizin, J.; Fuchs, M.; Awan, A.A.; Ahmad, I.; Akhtar, S.S.; Sadiq, S.; Razzak, A.; Weggenmann, D.; Fawad, F.; Khalid, N.; et al. Statistical landslide susceptibility assessment of the Mansehra and Torghar districts, Khyber Pakhtunkhwa Province, Pakistan. *Nat. Hazards* **2017**, *89*, 757–784. [CrossRef]
60. Youssef, A.M.; Pourghasemi, H.R.; El-Haddad, B.A.; Dhahry, B.K. Landslide susceptibility maps using different probabilistic and bivariate statistical models and comparison of their performance at Wadi Itwad Basin, Asir Region, Saudi Arabia. *Bull. Eng. Geol. Environ.* **2016**, *75*, 63–87. [CrossRef]
61. Aghdam, I.N.; Pradhan, B.; Panahi, M. Landslide susceptibility assessment using a novel hybrid model of statistical bivariate methods (FR and WOE) and adaptive neuro-fuzzy inference system (ANFIS) at southern Zagros Mountains in Iran. *Environ. Earth Sci.* **2017**, *76*, 237. [CrossRef]
62. Kornejady, A.; Ownegh, M.; Rahmati, O.; Bahremand, A. Landslide susceptibility assessment using three bivariate models considering the new topohydrological factor: HAND. *Geocarto Int.* **2017**, *33*, 1155–1185. [CrossRef]
63. Mahalingam, R.; Olsen, M.J.; O'Banion, M.S. Evaluation of landslide susceptibility mapping techniques using lidar-derived conditioning factors (Oregon case study). *Geomat. Nat. Hazards Risk* **2016**, *7*, 1884–1907. [CrossRef]
64. Samodra, G.; Chen, G.; Sartohadi, J.; Kasama, K. Comparing data-driven landslide susceptibility models based on participatory landslide inventory mapping in Purwosari area, Yogyakarta, Java. *Environ. Earth Sci.* **2017**, *76*, 184. [CrossRef]
65. Teeuw, R.M.; Leidig, M.; Saunders, C.; Morris, N. Free or low-cost geoinformatics for disaster management: Uses and availability issues. *Environ. Hazards* **2012**, *12*, 112–131. [CrossRef]
66. Leidig, M.; Teeuw, R.M.; Gibson, A.D. Data poverty: A global evaluation for 2009 to 2013—Implications for sustainable development and disaster risk reduction. *Int. J. Appl. Earth Obs. Geoinf.* **2016**, *50*, 1–9. [CrossRef]
67. Soldati, M.; Corsini, A.; Pasuto, A. Landslides and climate change in the Italian Dolomites since the Late glacial. *Catena* **2004**, *55*, 141–161. [CrossRef]
68. Valenzuela, P.; Iglesias, M.; Dominguez-Cuesta, M.J.; Garcia, M.A.M. Meteorological patterns linked to landslide trig-gering in Asturias (NW Spain): A preliminary analysis. *Geosciences* **2018**, *8*, 18. [CrossRef]
69. Uyeturk, C.E.; Huvaj, N.; Bayraktaroglu, H.; Huseyinpasaoglu, M. Geotechnical characteristics of residual soils in rain-fall-triggered landslides in Rize, Turkey. *Eng. Geol.* **2020**, *264*, 105318. [CrossRef]